Cascaded Speed Control of a PMSM for Electric Vehicles Using Non-Linear Model Predictive Control Incorporating GA-Tuned PI Current Control

Getiye Abule Shewangizaw

A Thesis Submitted to

The Department of Electrical Power and Control Engineering,

College of Electrical Engineering and Computing

Presented in Partial Fulfillment of the Requirement for the Master of Science Degree in Electrical Power and Control Engineering (Control Engineering)

Office of Graduate Studies

Adama Science and Technology University

May, 2025

Adama, Ethiopia

Cascaded Speed Control of a PMSM for Electric Vehicles Using Non-Linear Model Predictive Control Incorporating GA-Tuned PI Current Control

Getiye Abule Shewangizaw

Advisor: Dr. Endalew Ayenew

Co-Advisor: Mr. Iyuel Endale

A Thesis Submitted to

The Department of Electrical Power and Control Engineering,

College of Electrical Engineering and Computing

Presented in Partial Fulfillment of the Requirement for the Master of Science Degree in Electrical Power and Control Engineering (Control Engineering)

Office of Graduate Studies

Adama Science and Technology University

May, 2025

Adama, Ethiopia

DECLARATION

I hereby declare that this Master thesis entitled "**Cascaded Speed Control of a PMSM for Electric Vehicles Using Non-Linear Model Predictive Control Incorporating GA-Tuned PI Current Control**" is my original work and has not been submitted to any university for a similar purpose. The reference used in this thesis are duly recognized by appropriate citations.

Getiye Abule	__________	__________
Name of student	Signature	Date

RECOMMENDATION OF ADVISOR

We hereby certify that we have closely advised the student while developing this thesis and read the revised version of the thesis entitled "**Cascaded Speed Control of a PMSM for Electric Vehicles Using Non-Linear Model Predictive Control Incorporating GA-Tuned PI Current Control**" prepared under our guidance by Getiye Abule. Therefore, we recommend the submission of the thesis to the department following the applicable procedures.

Dr. Endalew Ayenew	__________	__________
Major Advisor	Signature	Date
Mr. Iyuel Endale	__________	__________
Co-Advisor	Signature	Date

APPROVAL SHEET

We hereby certify that the recommendation and suggestion given by the thesis review committee are appropriately incorporated into the final thesis entitled "**Cascaded Speed Control of a PMSM for Electric Vehicles Using Non-Linear Model Predictive Control Incorporating GA-Tuned PI Current Control**" by Getiye Abule.

Dr. Endalew Ayenew	__________	__________
Major Advisor	Signature	Date
Mr. Iyuel Endale	__________	__________
Co-Advisor	Signature	Date

APPROVAL OF BOARD OF REVIEWER

We, the undersigned, members of Board of the Reviewers of open defense by Getiye Abule have read and evaluated the thesis entitled "**Cascaded Speed Control of a PMSM for Electric Vehicles Using Non-Linear Model Predictive Control Incorporating GA-Tuned PI Current Control**" and assessed the understanding of the candidate about the proposed research. This is, therefore to certify that the thesis is accepted for partial fulfillment of the requirement of the degree of science in Electrical Power and Control Engineering (Control Engineering).

Chairperson	Signature	Date
Internal Examiner	Signature	Date
Dr Beteley Teka Hailu		June 05,2025
External Examiner	Signature	Date

Final approval and acceptance of the thesis is contingent upon the submission of its final copy to the Office of Post Graduate Studies (OPGS) through the Department Graduate Council (GDC) and School Graduate Committee (SGC).

Department Head	Signature	Date
Dean	Signature	Date
Office of Post Graduate Studies, Dean	Signature	Date

ACKNOWLEDGMENT

First and foremost, I would like to express my gratitude to Almighty GOD for endowing me with the strength to complete this work. I am very grateful to my advisor, Dr. Endalew Ayenew, for his invaluable guidance and comments throughout my thesis. His wisdom, critical suggestions, and inspiration at all moments have contributed immensely to shaping this research.

I would also like to take this chance to deeply thank my co-advisor, Mr. Iyuel (MSc.), for his patience, good attitude, and highest quality technical support in operating the nonlinear MPC MATLAB code. Simulation would not have been possible without his assistance.

I am also highly grateful to Mr. Minyamer Gelawe (MSc.), for his very helpful guidance and for helping me gain a clearer idea of my research subject, from the selection of the thesis title. I also use this moment to thank the Department of EPCE for providing necessary facilities, such as use of the computer lab, and for the arrangements that allowed me to conduct my research work.

Finally, my heartfelt thanks go to my family and friends for their unwavering support and patience throughout this long process. Their belief in me and constant encouragement provided me with the inspiration to keep going.

Table of Contents

ABSTRACT

As the world's transition to sustainable transport accelerates, Electric Vehicles (EVs) are now a vital solution to reduce carbon emissions and fossil fuel dependence. However, their energy efficiency and performance often degrade under varying load and road conditions. This problem of EV performance has to be optimized through the proper use of advanced motor types and the implementation of efficient control strategies. Among various motor types, the Permanent Magnet Synchronous Motor (PMSM) is chosen due to its small size, reliability, and high efficiency, which are ideal for EV applications. The Interior Permanent Magnet Synchronous Motor (IPMSM) is chosen in particular due to its greater torque density and efficiency at low speeds, which are critical for urban and dynamic driving conditions. For speed control of the IPMSM in this thesis, Nonlinear Model Predictive Control (NMPC) is applied due to its ability to control complex system dynamics and constraints effectively while resulting in high energy efficiency as well as optimal performance. Unlike other traditional control algorithms, NMPC facilitates better handling of nonlinearities and input-output constraints, and therefore it is very suitable for EVs under different driving conditions. *This research involved intensive examination of Hyundai Ioniq's resistive forces, power requirements, and torque requirements in the selection of proper motor parameters. NMPC in outer loop speed control and a Proportional-Integral (PI) controller whose parameters are tuned with the aid of a Genetic Algorithm (GA) for inner current control is employed as the control strategy. This control method is contrasted with a linear MPC for speed control and a GA-tuned PI controller for current control. In the comparison, NMPC achieves better performance with zero steady-state error and higher efficiency, while LMPC shows a steady-state error of 1.5469. The control and drive systems were simulated and implemented using MATLAB software.*

Keywords: NMPC, Hyundai Ioniq, IPMSM and PI-GA

LIST OF TABLES

LIST OF FIGURES

ACRONYMS

AC	Alternating Current
BLDCM	Brushless Direct Current Motor
CPSR	Constant Power Speed Range
DC	Direct Current
EV	Electric Vehicle
GA	Genetic Algorithm
ICE	Internal Combustion Engine
IM	Induction Motor
IPMSM	Interior Permanent Magnet Synchronous Motor
IPOPT	Interior Point OPTimizer
MPC	Model Predictive Control
NLP	Non-Linear Programming
NMPC	Non-Linear Model Predictive Control
OCP	Optimal Control Problem
PI	Proportional Integral
RK4	Range Kutta Fourth Order
SPMSM	Surface Permanent Magnet Synchronous Motor
SVPWM	Space Vector Pulse Width Modulation

CHAPTER ONE

INTRODUCTION

1.1 Background of the Study

The worldwide movement towards Electric Vehicles (EVs) has ensured that new and improved drive systems were invented to reduce carbon footprints and dependence on non-renewable resources. Among all kinds of motors, Permanent Magnet Synchronous Motors (PMSMs) have been the choice of EV manufacturers worldwide since they are more efficient, compact, and possess better torque density than brushless DC and induction motors (Gao et al., 2018). Therefore, the majority of automakers are turning towards PMSMs to meet demanding energy efficiency and performance requirements of modern EVs.

In particular, Interior Permanent Magnet Synchronous Motors (IPMSMs) are now favored because of their strength in maintaining efficient operation with a wide operating speed range and hence being suitable for different kinds of driving styles in urban as well as freeway conditions (Li et al.,2019). Their enhanced torque characteristics and flux-weakening capability bring significant advantage compared to Surface Permanent Magnet Synchronous Motors (SPMSMs) in dynamic automotive electric drive like the Hyundai Ioniq. However, IPMSMs come with challenges in terms of nonlinear dynamics, magnetic saturation, and field-weakening, which call for sophisticated control strategies.

Traditional control methods like Proportional-Integral (PI) controllers are widely used for their simplicity but are limited in handling the nonlinear nature of IPMSMs under varying loads and operating conditions (Lee et al., 2009). While Linear Model Predictive Control (MPC) provides greater flexibility, its reliance on linearization results in suboptimal performance when dealing with system nonlinearities. In contrast, Nonlinear MPC (NMPC) offers superior handling of dynamic constraints and nonlinear behaviors, enabling accurate torque and speed control with improved energy efficiency. In this thesis, the inner current loop of the IPMSM in the Hyundai Ioniq is regulated using a PI controller whose parameters are optimized via a Genetic Algorithm (GA). This two-layer control approach enhances system robustness and adaptability to dynamic operating conditions. Furthermore, the study includes a comprehensive analysis of resistive forces, power demands, and torque requirements of the Hyundai Ioniq to assess the effectiveness of the proposed control strategy in advancing EV drive systems globally.

The excellence of the presented approach is attested by comparative comparison with traditional linear MPC control and showing the future potential of NMPC in revolutionizing the performance of electric vehicles in demanding and diversified applications.

1.2 Statement of the problem

The electric drive system in Electric Vehicles (EVs) is a highly critical piece of technology that transforms electrical energy into mechanical motion with efficiency, reliability, and response characteristics under varying driving loads. The motors like Induction Motors (IMs) and Brushless DC motors (BLDCM) are limited by lower efficiency, lower torque density, and inability to scale for varying loads. Interior Permanent Magnet Synchronous Motors (IPMSMs) are now a better choice with better efficiency, torque behavior, and flux-weakening capability. IPMSMs have been gaining popularity in industry now, e.g., Hyundai Ioniq. However, IPMSMs are also very difficult in nature due to their inherent non-linearities such as magnetic saturation and field-weakening effects. Traditional control techniques, like Linear Model Predictive Control (MPC), are not effective in the presence of such complexities, particularly under dynamic operating conditions with sudden changes in operating points. To combat such challenges, the current research puts forward a Non-Linear Model Predictive Control (NMPC) method for IPMSM speed control that can effectively address non-linearities and system limitations. Compared to Linear MPC, NMPC directly models the dynamics of the system and optimizes control actions in real time, ensuring stability and efficiency under varying load conditions. Additionally, a PI controller whose parameters are optimized with GA is utilized in the inner current loop that enhances the regulation of current and makes the system more flexible.

The proposed control framework combines NMPC's precision in managing IPMSM dynamics with GA-tuned PI’s robustness for current control, ensuring energy-efficient and reliable performance. This approach, is tested on a Hyundai Ioniq-based EV model, aims to validate the effectiveness of this dual-layer control strategy, providing a robust solution for the challenges in modern EV drive systems.

1.3 Objective

1.3.1 General Objective:

The general objective of the thesis is to study and develop cascaded speed controller for a PMSM using Non-Linear Model Predictive Control incorporating GA-tuned PI current control for Hyundai Ioniq Electric Vehicle case.

1.3.2 Specific Objectives:

- Analyzing force, power and torque requirement of the vehicle in the case of Hyundai Ioniq car to select an appropriate IPMSM.
- Develop a mathematical model of the IPMSM.
- Design and implement Non-Linear Model Predictive Control (NMPC) for speed control.
- Optimize inner loop PI current controllers using a Genetic Algorithm (GA).
- Evaluate the performance of the proposed control system by using MATLAB software package.
- Performance comparison of the proposed NMPC GA-PI controller with linear MPC.

1.4 Scope of the study

The thesis is designed on the simulation design and mathematical modeling of Hyundai Ioniq vehicle dynamics and Interior Permanent Magnet Synchronous Motor. MATLAB software is utilized in the simulation of NMPC based speed and current control of IPMSM motor for the purpose of propulsion in electric vehicle (Hyundai Ioniq) application. Methods of IPMSM motor drives are developed and discussed for performance in both current controller methods as well as in speed controller methods.

1.5 Significance of the Study

Global and global concerns of energy wastage and air pollution are making the world undergo a shift from rapidly growing non-renewable energy sources to clean, renewable ones. The renewable sources are environmentally friendly and are gaining momentum in most nations against such pressing issues. Of specific importance is the adoption of it by the ASTU Center of Transportation and Vehicle Engineering (CTVE) and the E-Bajaj Center of Excellence as they are actually engaged in creating and producing electric vehicles with design specifications appropriate to the Ethiopian market.

1.6 Limitation of the Study

This thesis focuses on regulating the speed and current of Interior Permanent Magnet Synchronous Motor (IPMSM) in an Electric Vehicle (EV) system. The validation of the proposed control strategy was conducted exclusively through simulation in the MATLAB environment. While this approach enables comprehensive performance analysis under various operating conditions, it does not account for non-idealities and uncertainties inherent in real-world hardware implementations, such as sensor noise, inverter nonlinearities, or thermal effects.

1.7 Thesis Organization

This thesis work is organized in six chapters.

Chapter 1: Background of the study, problem statement, objective, scope and significance

of the study are clearly described.

Chapter 2: The background of EVs, trends of common electric motors for EVs and related recent research papers are well reviewed and explained in this chapter.

Chapter 3: Analyzing of the dynamic model of the Hyundai Ioniq car through free body diagram and mathematical model of PMSM are clearly derived in this chapter.

Chapter 4: This chapter contains Controller design.

Chapter 5: Simulation result is analyzed and discussed in this section.

Chapter 6: In this section, conclusion and recommendation are illustrated.

CHAPTER TWO

LITERATURE REVIEW

2.1 Theoretical Background of Electric Vehicle

Robert Anderson constructed the first electric vehicle in 1839, and subsequently, there was David Salomon's 1870 electric vehicle with a light electric motor (Minyamer, 2020). The initial electric vehicles (EVs) suffered from poor performance due to the heavy batteries. As the technology of batteries upgrade EVs are now a game-changer product to address the environmental and energy issues posed by traditional Internal Combustion Engine (ICE) vehicles. Based on electricity stored in batteries, EVs eliminate tailpipe emissions to zero, reduce fossil fuel consumption, and offer maximum energy efficiency. The electric motor is the core of an EV's drive system, pumping electrical energy into mechanical torque to drive the wheels (Cao et al.,2019). Among the numerous motor technologies available for use, Permanent Magnet Synchronous Motors (PMSMs) are the most popular option among newer-generation EVs due to their improved performance characteristics.

From the discovery of interior-rotor PM synchronous motors, a significant performance, efficiency, and practicality leap was experienced in EV development. Unlike previous motors having their faults, an unfavorable power density, unsharp torque control, or efficiency at different speeds, it will have an excellent power density, sharp torque control, and good efficiency-the very qualities needed in the trending application of EVs. In the early 2000s, large automotive manufacturers like Toyota, Nissan, and Hyundai started adopting IPMSMs in their EV and hybrid projects, convinced of the implicit advantages relating to energy savings and compact design of these motors (Rauth et al.,2020). This development in turn paved the way for more reliable and longer-range electric vehicles, and consequently, from being split into niche-way-to-low-speed vehicles or vans to being accepted by the general public as means of transport. It is evident that IPMSMs have led to the relatively fast growth of the EV industry and hence supported the worldwide drive for sustainable mobility on these lines: enabling high-performance, energy-efficient electric drivetrains.

2.2 Electric Motor Varieties

Induction, DC, PMSM, and switched reluctance motors are among the electric motor types used or studied for electric vehicle applications. PMSMs are used quite frequently because they exhibit very high efficiency. Rotor windings are removed with PMSMs, so copper losses are also removed. There is no commutator, so maintenance is very low, and power density of PMSMs is quite high. Figure 2.1 below presents a grouping of electric motors according to power supply and operating features.

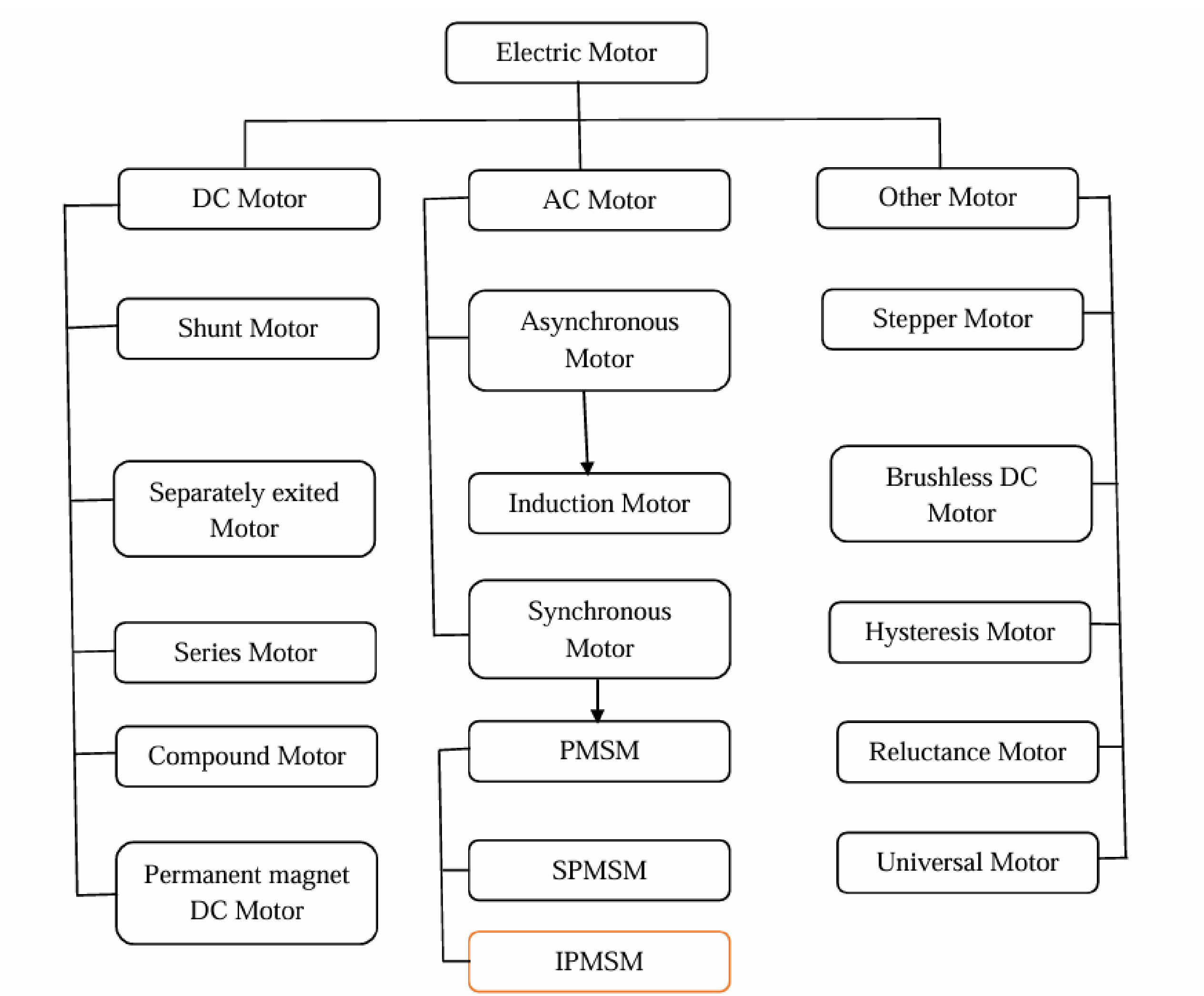

Figure 2.1 Drive systems classification according to their power source and performance behavior (Thattil et al,.2019).

2.2.1 AC Induction Motor (IM)

In an induction motor, a sinusoidal AC stator winding current produces a rotating magnetic field. The rotating magnetic field causes the rotor bars to induce a current, which produces a magnetic field of its own. Stator and rotor magnetic fields rotate at varying frequencies (generally, the stator's frequency, ω_s, is higher than the rotor's, ω_r), resulting in torque development.

Figure 2.2 Induction motor with stator and rotor (generated by AI, 2025).

2.2.2 Brushless DC Motor

Brushless DC (BLDC) motors, which are commutated electronically, are an improvement over traditional brushed DC motor. As synchronous motors powered by a DC source, they typically consist of permanent magnets moving with respect to a stationary armature. BLDC motors have several advantages, such as high speed, high efficiency, low maintenance, and precise speed and torque control. Their compactness facilitates high power density and efficiency compared to other motors (Rauth et al,. 2020). BLDC motors have limitations however, their torque is compromised at higher speeds with heavy loads, constraining their high-power applications. They also induce vibration and noise due to torque ripple.

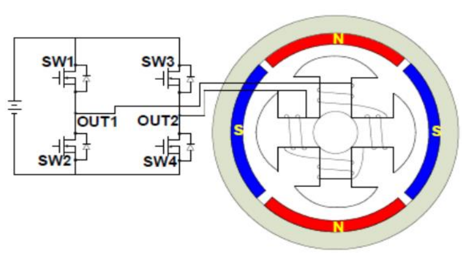

Figure 2.3 Brushless DC Motor Illustration (Liu, 2008).

2.2.3 Permanent Magnet Synchronous Motor (PMSM)

PMSM has a permanently mounted magnet on the rotor and three-phase AC winding on the stator. The PMSM is built in the same way as synchronous motor but with no field winding on the rotor side of the PMSM. Sinusoidal form AC current supplies the PMSM.

The structure of Figure 2.4 (a) shows the surface-mounted PMSM, this structure possesses maximum air gap flux density because it is in direct contact with the air gap. The quadrature axis to direct axis inductance variation in this machine is very minimal. Figure 2.4 (b) shows the interior PMSM the magnet is placed at the rotor lamination's center. The IPMSM is robust from a mechanical point of view and suitable for high-speed applications (Krishnan, 1991).

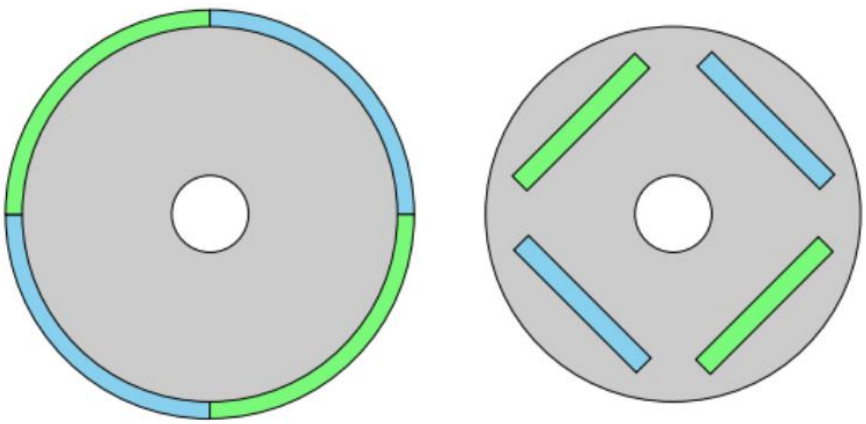

(a) (b)

Figure 2.4 Schematic of SPMSM and IPMSM Configurations (baral et al., 2021).

SPMSM and IPMSM lies in their cogging torque and acoustic noise behaviors. SPMSMs typically exhibit higher cogging torque owing to the stronger, more localized magnetic interactions between the surface-mounted magnets and stator teeth. This may generate noticeable torque ripple and vibration, especially at low speed or startup conditions, which results in greater acoustic noise.

On the other hand, IPMSMs with built-in magnets possess a more dispersed magnetic field, reducing the cogging torque and smoothening the production of torque. This not only minimizes vibration but also leads to quieter operation. The extra reluctance torque in IPMSMs also renders them better performers, making them ideal for electric vehicle or robotics applications where low noise, lower vibration, and smooth control are desired.

Table 2.1 Comparison between BLDC motors and PMSM (Derammelaere et al., 2016) (*Bello et al., 2014*).

Feature	BLDC Motor	PMSM	Advantages of PMSM
Working Principle	Trapezoidal back EMF, electronic commutation	Sinusoidal back EMF, electronic commutation	Smoother operation and better torque control
Control Complexity	Simple control with trapezoidal commutation	Complex control due to sinusoidal commutation (FOC, MPC)	Advanced control enables precise speed and torque regulation
Torque Ripple	High due to trapezoidal commutation	Lower due to sinusoidal commutation	Reduces vibration, improves efficiency and ride comfort
Efficiency	Lower due to higher losses and ripples	Higher efficiency due to smoother operation	Better energy efficiency, reducing power consumption
Power Density	Moderate	Higher power density due to smooth torque production	More power output for the same motor size
Speed Range	Limited at high speeds due to back EMF distortion	Wide speed range, better high-speed performance	Suitable for high-speed EV applications
Noise & Vibration	Higher due to commutation switching	Lower due to sinusoidal waveform	Quieter operation, reducing vehicle noise
Regenerative Braking	Less efficient	More efficient, better energy recovery	Improves battery life and extends driving range
Cost	Lower manufacturing cost	Higher cost due to advanced control requirements	Higher cost justified by better performance and efficiency
Applications	Mostly used in Household appliances, fans, drones, power tools	Mostly used in Electric vehicles, industrial automation, robotics	Ideal for EVs due to superior performance characteristics

Table 2.2 Comparison between SPMSM and IPMSM (Lu et.,2024) (Murakami et., 1999).

Feature	SPMSM (Surface-Mounted PMSM)	IPMSM (Interior PMSM)	Advantages of IPMSM
Magnet Placement	Magnets are mechanically fastened to the rotor surface.	Magnets are integrated within the rotor assembly.	Better mechanical stability and durability
Saliency Effect ($L_d \approx L_q$)	Low ($L_d \approx L_q$)	High ($L_d < L_q$)	Enables reluctance torque, improving efficiency
Torque Production	Only uses electromagnetic torque	Uses both electromagnetic and reluctance torque	Higher torque output for the same input power
Efficiency	Lower due to no reluctance torque contribution	Higher due to additional reluctance torque	Reduces energy consumption in EVs
Maximum Speed	Limited by magnet adhesion strength	Higher due to improved mechanical stability	Suitable for high-speed EV applications
Flux Weakening Capability	Limited	Strong	Allows operation at a wider speed range
Torque Ripple	Lower	Higher	Trade-off, but can be mitigated with advanced control
Mechanical Strength	Weaker, risk of magnet detachment at high speeds	Stronger due to embedded magnets	More robust for high-speed and high-power applications
Manufacturing Cost	Lower	Higher due to complex rotor design	Higher cost justified by better performance
Applications	Industrial automation, robotics, some EVs	Electric vehicles, high-performance applications	More suitable for modern EV powertrains

2.3 Review of Related Works

A summary of literatures published regarding the speed control of PMSM with and without electric vehicle is reviewed as follows.

In (Liu et al., 2019), Explicit MPC (EMPC) is proposed to control IPMSM in electric vehicles. EMPC linearizes the model with voltage compensation to ease nonlinear dynamics and combines speed and current control in a single structure for increased computational efficiency using a binary search-based optimization strategy. While this strategy effectively reduces the computational load, it accomplishes this at the cost of model accuracy through the use of simplifications. It can be improved by employing Non-Linear MPC (NMPC) for speed control, which enjoys direct management of the system nonlinearities and no linearization, offering more model accuracy and flexibility. Inner-loop current control is also can be optimized with a GA-tuned PI controller, complete with an uncompromising cascaded structure and improved energy efficiency Id current.

In (Mulugeta, 2024), a Model Predictive Control (MPC) method was introduced for speed regulation of a permanent magnet synchronous motor (PMSM) for electric vehicle (EV) drives, in particular for the Hyundai ATOS vehicle. The strategy employed MPC as the outer-loop speed controller and a Genetic Algorithm (GA)-optimized Proportional-Integral (PI) controller as the inner-loop current controller, with input-output constraints and performance optimized relative to linear quadratic regulator (LQR) and GA-PI control. This linear Model Predictive Control (MPC) approach was developed for speed control of a surface mounted permanent magnet synchronous motor (SPMSM) in EV applications, but most vehicles currently use IPMSM which its mathematical equation is nonlinear and NMPC is required.

In (Tian et al., 2023), linearization of an input-output feedback is utilized for simplifying nonlinear dynamics of an IPMSM such that the cost function is linearized so that it is optimal for a linear predictive control technique. This technique cancels nonlinearity though, but it creates practical challenges due to the complexity involved in feedback linearization and fails to make maximum use of reluctance torque generated by the d- and q-axis asymmetrical inductances. Additionally, the predictive controllers lack the improvements in the form of torque-to-current ratio enhancement, rendering the control strategy more complicated and restricting its efficiency. These can be addressed by employing Non-Linear Model Predictive Control (NMPC) directly, which naturally accommodates the nonlinear nature of IPMSM without linearization. Further, a GA-tuned PI controller offers maximum current regulation and maximum utilization of reluctance torque, allowing for improved energy efficiency and torque control under varying conditions.

In (PC et al., 2024), Field-Oriented Control (FOC) technique was applied to surface-mounted PMSMs (SPMSMs) for EV drives. The FOC facilitated independent torque and flux control through PI controllers manually tuned. Though shown to be practicable in terms of hardware implementation, the FOC was implemented considering SPMSM, as opposed to IPMSM, thus ignoring nonlinearities and saliency effects. Additionally, the PI controllers were non-adaptive and not optimally tuned, resulting in suboptimal performance when dealing with varying EV driving conditions. In contrast, the proposed thesis tackles nonlinear IPMSM modeling, employs NMPC for speed control, and implements GA-based PI tuning of current loops, filling a fundamental performance and adaptability gap.

In (Tan et al.,2020) introduced an Interior Permanent Magnet Synchronous Motor (IPMSM) model predictive control (MPC) strategy for electric vehicles. It was designed upon a conventional control method (CCM)-based MPC with complete-speed domain control. Being familiar with the weaknesses of cascading MPC in dynamic response and MPC's multi-objective optimality inefficiency, they proposed a non-cascading MPC architecture. Simulation results of comparison between cascade and non-cascade MPC under various load torque and speed levels confirmed the superior dynamic performance of the non-cascading approach. One major drawback of this study is the absence of system constraint considerations.

(Nguyen et.al.,2024), identifies a cascaded control structure where MRAC is applied to the speed loop. It ensures stability according to the Lyapunov theorem and manages parameter uncertainties such as resistance and inertia and achieves robust disturbance rejection and high dynamic response. However, MRAC relies on pre-specified reference models, thereby sacrificing its ability to cope with non-linearities such as magnetic saturation in IPMSMs.

(X. Huang et al., 2020) proposes a double MPC strategy for managing the speed and current of a PMSM system. The speed is controlled via an outer-loop MPC, while the current is controlled using an inner-loop deadbeat prediction controller. The study confirms that the approach results in no overshoot, faster response, enhanced steady-state performance, and enhanced disturbance rejection in comparison to traditional PI-speed and deadbeat-current control. Even though the double MPC approach achieves significant improvement in relation to traditional methods, it does not exploit fully the nonlinearities and complex dynamics associated with IPMSMs such as magnetic saturation and non-stationary load conditions.

In (K. Zhang et al., 2022), an adaptive nonlinear predictive control algorithm is proposed for IPMSM in the presence of parameter uncertainties and real-time disturbances. The approach integrates disturbance observers and real-time parameter estimation into an NMPC framework, allowing it to self-adjust control actions based on system variation. These yields improved robustness under highly dynamic EV conditions and offers higher energy efficiency. However, the algorithm requires high computational capacity and may suffer from delays in embedded environments.

(Gao et al., 2018) proposed a non-cascaded MPC architecture for IPMSM drives in electric vehicles, which aims to improve dynamic response by combining speed and current control within a single controller. This approach departs from traditional cascaded structures, where speed control is the outer loop and current control is the inner loop. While this non-cascaded MPC offers the advantage of a more integrated design, it may not fully address the optimization of the inner current control loop itself. Specifically, it does not incorporate advanced techniques like Genetic Algorithms (GAs) to fine-tune the current control parameters for enhanced performance and efficiency. Furthermore, the study does not explicitly consider the minimization of energy consumption, a critical factor in EV applications. Therefore, a potential modification, and a key contribution of this thesis, is to integrate GA-tuned PI controllers within an NMPC framework. This would retain the benefits of NMPC in handling system nonlinearities, while also optimizing the inner current control loop for improved dynamic response, torque control, and energy efficiency.

In (El Fakir et al., 2023) an adaptive backstepping-based controller is developed to handle uncertainties and nonlinearities in PMSMs. Though effective, this method lacks a predictive horizon and cannot optimize control actions over future time intervals. But NMPC anticipates future states and makes optimal decisions over a horizon, outperforming backstepping in terms of foresight and constraint handling. This thesis leverages this advantage and enhances current regulation using GA tuning.

In (Liu et al., 2016), addresses the speed control problem for Permanent Magnet Synchronous Motor (PMSM) drive systems. It notes that while predictive control offers fast transient response, its performance can degrade with model uncertainties and load disturbances. To improve robustness, the paper proposes a control method that combines generalized predictive control with a high-order terminal sliding mode controller. The high-order terminal sliding mode controller is designed to reduce chattering, a common issue in traditional sliding mode control. The stability of the system with the proposed controller is proven. Simulation results are presented to verify the effectiveness of the control method. While this paper presents a robust control method for PMSMs, it primarily focuses on speed control. It does not explicitly address the optimization of the inner current control loop, which is critical for overall system performance. Additionally, the paper does not explicitly consider minimizing energy consumption, an important factor in EV applications.

In (Wang & Yu, 2023), a Fuzzy Model Predictive Control (FMPC) method was shown for Permanent Magnet Synchronous Motor (PMSM) speed regulation. Robustness and quality of prediction under uncertainty, along with a smooth tracking response, were aided by the fuzzy logic. But the FMPC was intended for common industrial PMSM operations and did not consider electric vehicle (EV) dynamics, let alone the nonlinearities involved with interior PMSMs (IPMSMs). Apart from that, the current control was controlled by ordinary PI controllers with no optimization method such as Genetic Algorithms (GA), resulting in non-optimal dynamic performance. This presents a research gap to a control scheme that utilizes nonlinear MPC for IPMSM speed control and GA-optimized PI controllers for inner-loop current control, both realized in this study.

In (Ruan et al., 2025), an Adaptive High-Order Non-Singular Fast Terminal Sliding Mode Controller (AHONFTSMC) was considered for position regulation of PMSMs with stability and fast convergence. While the method in question addressed model uncertainty and disturbances to a great degree, the point of consideration remained position regulation as opposed to speed control under EV drive cycles. Moreover, the controller used already was conventional in nature, as opposed to utilization of optimization procedures like Genetic Algorithms. The switching at high frequencies also had the possibility of leading to chattering, which would reduce system life. Compared to this approach, this work utilizes NMPC for optimizing speed tracking with constraints and incorporates GA-tuned PI control for better regulation of torque and current two aspects that are absent in Ruan's research.

Table 2.3 Literature review summary.

Title	Authors	Method	Achievement	Gap Addressed by this proposed
IPMSM Speed and Current Controller Design for Electric Vehicles Based on Explicit MPC	(Liu et al., 2019)	Explicit Model Predictive Control (EMPC) with voltage compensation and binary search optimization	Combined speed and current control in a single structure; reduced computational burden	Linearization compromises model accuracy; lacks GA-tuned inner current control; does not fully exploit IPMSM nonlinearities
Model Predictive Control of PMSM for Electric Vehicle Applications	(Mulugeta, 2024)	Linear MPC as outer-loop speed controller with GA-optimized PI inner-loop current controller	Improved performance over LQR and GA-PI control; applied to SPMSM in EVs	Applicable to SPMSM; does not address IPMSM nonlinearities; lacks NMPC implementation
Field-Oriented Control of SPMSM for Electric Vehicle Drives	(PC et al., 2024)	Field-Oriented Control (FOC) with manually tuned PI controllers	Achieved independent torque and flux control; practical hardware implementation	Focused on SPMSM; PI controllers not optimally tuned; does not consider IPMSM saliency and nonlinearities
Non-Cascaded Model Predictive Control for IPMSM Drives in Electric Vehicles	(Gao et al., 2018)	Integrated speed and current control using non-cascaded MPC architecture	Improved dynamic response by combining control loops	Does not optimize inner current control loop; lacks GA tuning; energy efficiency considerations are limited

Adaptive Nonlinear Predictive Control for IPMSM with Parameter Uncertainties	(K. Zhang et al., 2022)	Adaptive NMPC incorporating disturbance observers and real-time parameter estimation	Enhanced robustness under dynamic conditions; improved energy efficiency	High computational requirements; lacks GA-tuned PI controller for inner-loop current control
Adaptive Backstepping Control for PMSM	(El Fakir et al., 2023)	Adaptive backstepping control with Lyapunov-based design	Accurate rotor speed tracking; robust against parameter variations and disturbances	Lacks predictive horizon; does not optimize control actions over future intervals; inner-loop current control not addressed
Fuzzy Controller-Based Predictive Speed Control of a Permanent Magnet Synchronous Motor	(Wang & Yu, 2023)	Fuzzy Model Predictive Control (FMPC)	Robust speed tracking under uncertainty; smooth response	Designed for industrial PMSM applications; does not consider EV dynamics or IPMSM nonlinearities; lacks GA optimization for current control

Generally, most of the above reviewed articles rely on linearization, limiting their ability to capture the full nonlinear motor dynamics. Some are aimed at non-EV applications, some overlook inner-loop current control, and some use SPMSMs, which are simpler but less efficient for EVs than IPMSMs. This thesis resolves such limitations with the application of Nonlinear Model Predictive Control (NMPC) for outer-loop speed control and system nonlinearities and future-state estimation. An inner current loop is controlled using a Genetic Algorithm (GA)-tuned PI controller to realize fast and robust response. The dual design has improved constraint handling, energy efficiency, and tracking capability, especially under low-speed and dynamic driving conditions where IPMSM nonlinearity and saliency are most challenging.

CHAPTER THREE

METHODOLOGY

3.1 Introduction

This chapter clearly outlines the materials, techniques, and methods used in this study. It covers the vehicle dynamics analysis and the mathematical modeling of the Interior Permanent Magnet Synchronous Motor (IPMSM) drive. In general, it outlines the methodological approach taken to achieve the research objectives, which aim at designing and implementing an advanced speed and torque control strategy for an Interior Permanent Magnet Synchronous Motor (IPMSM) used in a Hyundai Ioniq electric vehicle (EV).

3.2 Materials

To evaluate and validate the suggested control approach, simulations were conducted using MATLAB software. MATLAB code was created for the purpose of:

- Simulate power Vs speed characteristics of the vehicle.
- Design and tune the outer-loop NMPC and inner-loop PI controllers.
- Compare the performance of the proposed control strategy with linear MPC techniques.

For the execution of the NMPC controller, open-source software packages such as CasADi and IPOPT are utilized.

CasADi is a symbolic automatic differentiation and optimization framework that offers efficient tools for nonlinear optimization problem formulation and solution.

IPOPT is a state-of-the-art large-scale nonlinear optimization problem solver that can handle intricate objectives and constraints. With these sophisticated tools, the NMPC controller is successfully formulated and implemented.

Mathematical formulas and equations are displayed by MathType, and MS Office 2019 is utilized for document preparation.

3.3 Method of the system

To achieve objectives outlined in chapter one, the techniques and methods below were followed.

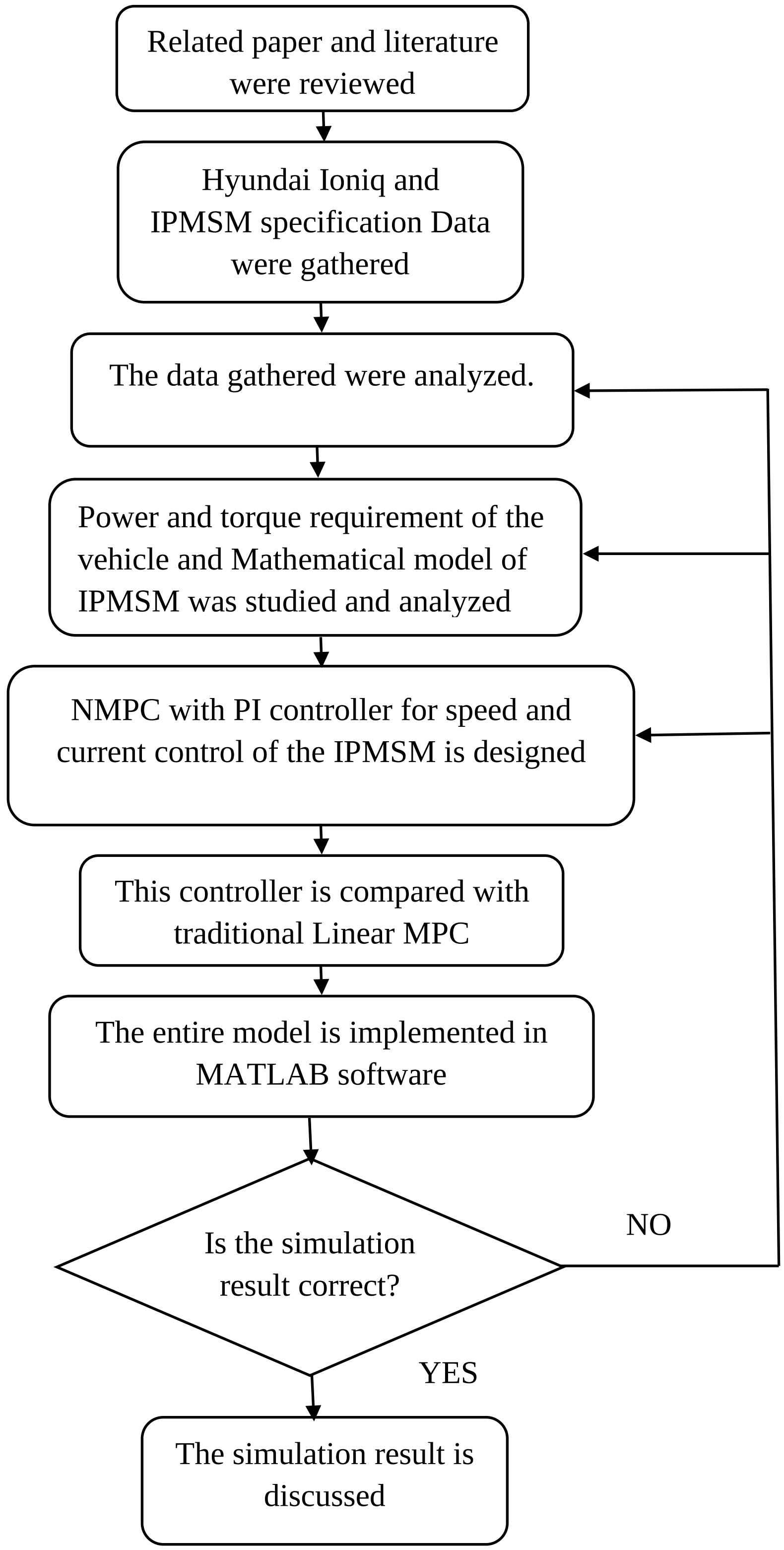

Figure 3.1 Research Methods Block Diagram.

3.4 Block diagram of proposed Method

Figure 3.2 illustrates the block diagram of NMPC-based speed control of an IPMSM drive in Hyundai Ioniq electric vehicle propulsion. The control system will regulate the difference between the reference speed(ω_{ref}) and measured speed(ω_m) by employing NMPC. The NMPC will predict the required I_q current based on the measured speed. In the proposed vector control technique, the I_d component is the current in the direct axis of the motor, which is parallel to the rotor magnetic field and it controls the magnetization level of the motor (and indirectly contributes to torque due to saliency in IPMSMs). This I_d produce reluctance torque in addition to electromagnetic torque as the d-axis Inductance (L_d) and q-axis Inductance (L_q) is not equal in this motor case.

The control method will regulate the I_q current to control motor torque so as to achieve independent speed and torque control. The control method will directly control motor speed and torque accurately by adjusting the I_q current as well as I_d current. The inner loop PI current controller will generate the V_d and V_q reference signals, which will be supplied to the Space Vector Pulse Width Modulation (SVPWM) as gate inputs in order to generate the corresponding switching signals. The six transistors of a three-phase inverter will use these signals in order to switch the DC supply to the required AC waveform for the motor.

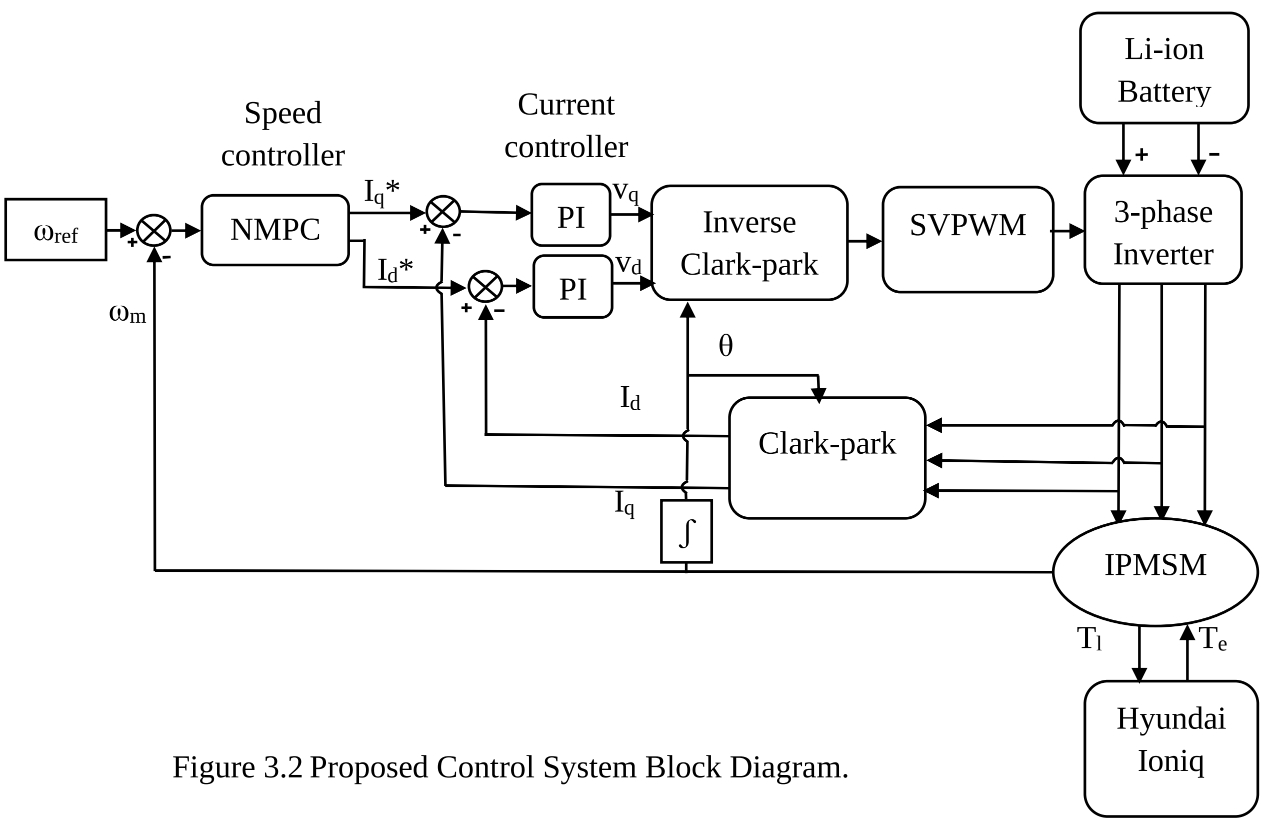

Figure 3.2 Proposed Control System Block Diagram.

3.5 Dynamic Analysis of the Hyundai Ioniq Electric Vehicle

The functioning of the Hyundai Ioniq EV is largely controlled by its powertrain, which includes the battery, drive motor, inverter, and the control systems. The most critical parts of the drivetrain are the battery and the IPMSM (Interior Permanent Magnet Synchronous Motor). Unlike traditional internal combustion engines, the Ioniq's powertrain eliminates complex mechanical components like the clutch and uses electric power transmission instead to achieve higher efficiency and reduce design complexity (Xin et al., 2017). The battery of the Hyundai Ioniq is a high-capacity lithium-ion polymer battery, and it is the primary source of power for propulsion. The power is supplied to the IPMSM through an inverter, which uses DC power as input and provides AC power for the motor drive. The motor's energy efficiency and torque density make the Ioniq as efficient in a range of speeds. Control systems, like speed controller and current controller, are crucial in determining maximum motor efficiency and performance.

3.5.1 Driving Force and Power in the Hyundai Ioniq EV

There are various forces that exert on the Hyundai Ioniq electric vehicle during its motion. In this study, the selection of the drive motor is according to the design requirements of the vehicle in relation to its dynamic response. The dynamic modeling of the Hyundai Ioniq considers road surfaces, wheel interactions, and positional characteristics of the vehicle. When the vehicle operates, it experiences forces like tire rolling resistance, aerodynamic drag, and gradient force on slopes as shown in the Figure 3.3.

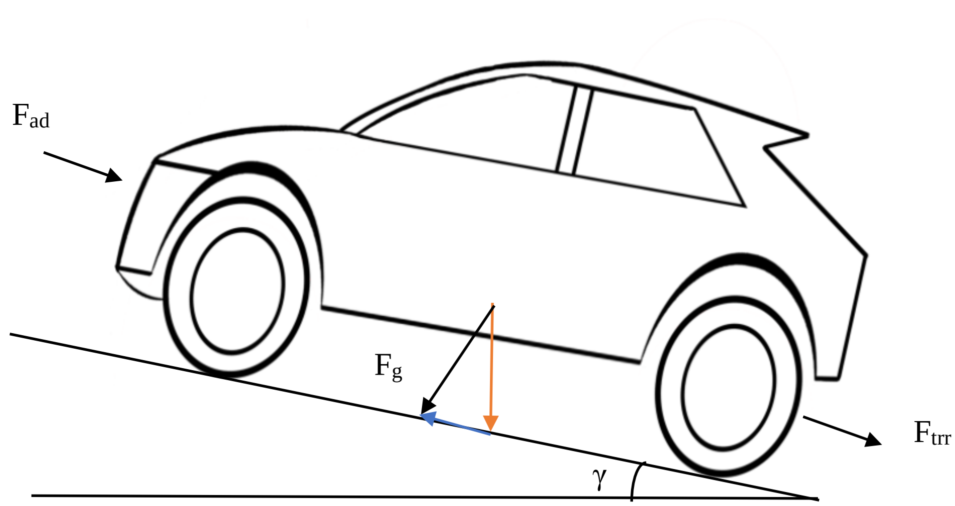

Figure 3.3 Free body diagram of Hyundai Ioniq Vehicle.

The combination of all these forces is the road load force, which plays an important role in the optimization of the motor and control system design.

$$F_T = F_{trr} + F_g + F_{ad} \tag{3.1}$$

Where, F_T is total force, F_{trr} is tire rolling resistance force, F_g is gradient force and F_{ad} is aerodynamic drag force.

Table 3.1 Hyundai Ioniq car specification (Hyundai Motor Company, 2023).

parameter	Symbol	Value
Speed	v	185 km/h
Gross weight	M	2600 kg
Width	W	1890 mm
height	H	1600 mm
Radius of the tire	r	0.37055 m
Coefficient of drag	C_{ad}	0.29
Transmission gear ratio	Gr	4.706

3.5.1.1 Force Due to Tire Rolling Resistance

The force due rolling resistance of a tire is an important factor to consider in vehicle dynamics, particularly for electric cars like the Hyundai Ioniq. The force arises due to the energy dissipation when the tires deform when rolling over a surface. It has a significant influence on the vehicle's energy usage, range, and overall performance.

It is expressed as:

$$F_{trr} = C_{trr} \times M \times g \times \cos(\gamma)$$

$$= 0.01 \times 2600\text{kg} \times 9.81 \frac{m}{s^2} \times \cos(11.30°) \quad (3.2)$$

$$= 250.1155\text{N}$$

Where, M is the gross mass of the Hyundai Ioniq car, g is the acceleration due to the gravity, C_{trr} is the tire rolling resistance coefficient (for concrete condition C_{trr}=0.01) the case of good contact surface is considered if the poor case is considered the force will be doubled. γ is angle of the inclination and the incline angle of **11.3°** was selected to simulate a **worst-case uphill driving scenario**, which is essential for evaluating the performance of the proposed speed control strategy under high-load conditions. This angle approximates the steepest gradients commonly encountered in real-world urban and mountainous roads.

The power (P_{trr}) needed to overcome the rolling resistance is determined by:

$$P_{trr} = F_{trr} \times \text{speed} \left(\frac{m}{\text{sec}}\right)$$

$$=250.1155\text{N} \times \frac{185000m}{3600\text{sec}} \quad (3.3)$$

$$=12.853KW$$

The coefficient of friction values for various surface types are presented in the Table 3.2.

Table 3.2 Coefficient of friction for different types of surfaces (Akhtar et al., 2015).

Contact surface	Coefficient of tire rolling resistance (C_{trr})
Concrete(good/fair/poor)	0.01/0.015/0.02
Asphalt(good/fair/poor)	0.012/0.017/0.022
Macadam (good/fair/poor)	0.015/0.022/0.037
Mud (firm/medium/smooth)	0.037/0.09/0.15
Sand (firm/soft/dune)	0.060/0.15/0.3

3.5.1.2 Gradient (Climbing) Resistance Force

The force necessary for driving a vehicle on an incline, referred to as the gradient force (F_g), is a critical component of vehicle dynamics. The gradient force is required to counteract the force of gravity on the vehicle as it travels up a slope. Both the weight of the vehicle and the slope angle dictate the magnitude of the gradient force. This thesis focuses on the examination of driving conditions uphill to test the performance of the vehicle.

$$F_g = M \times g \times sin(\gamma)$$

$$= 2600Kg \times 9.81 \frac{m}{s^2} \times \sin(11.30°) \tag{3.4}$$

$$= 4997.802\text{N}$$

where M represents the total mass of the vehicle and its cargo (in kilograms), g is the acceleration due to gravity (in meters per second squared), and γ is the road or hill-climbing angle, expressed as the road slope in radians.

The power demand to overcome the gradient force at a speed of 92.5 km/hr is:

$$P_g = F_g \times speed(\frac{m}{\text{sec}})$$

$$= 4997.802N \times (\frac{92500m}{3600\text{sec}}) \tag{3.5}$$

$$= 128.4157KW$$

3.5.1.3 Aerodynamic drag Force

A moving vehicle experiences aerodynamic drag, a force resisting its motion. This force of drags results from two major components:

- Skin Friction Drag: It occurs because of the friction between the air molecules and the surface of the vehicle.
- Form Drag: This is an effect of pressure differences created by the shape of the vehicle as it moves through the air.

The magnitude of the aerodynamic drag force (F_{ad}) depends on various parameters, including the vehicle's speed, frontal area, drag coefficient, and air density. The relationship among these parameters is usually given by:

$$F_{ad} = \frac{1}{2} C_{ad} \times A_f \times \varrho (V + Va)^2$$

$$= \frac{1}{2} \times 0.29 \times 2.5704 \times 1.23 (\frac{185000}{3600} + 0)^2 \quad (3.6)$$

$$= 1210.63N$$

Where, C_{ad} - coefficient of aerodynamic drag (its value is 0.29 from the vehicle specification),

A_f - frontal area of the vehicle calculated by: $A_f = 0.85 \times h \times w = 0.85 \times 1.89 \times 1.6 = 2.5704$ h and w - are the height and width of the vehicle respectively, V-vehicle speed and Va- speed of air assumed to be zero and ρ - the air density in $\frac{kg}{m^3}$ =1.23.

Hence, the air speed is less than the vehicle speed, and the power required to overcome it can be ignored. but the Aerodynamic drag power (P_{ag}) can be considered as a maximum of 1.5KW (Minyamer, 2020).

Therefore, the maximum power required from the IPMSM to drive the Hyundai Ioniq electric vehicle under all driving conditions i.e., the maximum tractive power required to drive the vehicle can be expressed as:

$$P_t = P_{trr} + P_g + P_{ag}$$

$$= 12.853 + 128.4157 + 1.5 \quad (3.7)$$

$$= 142.7687\text{kw}$$

The Equation for the mechanical output power required to propel the vehicle is:

$$P_m = \frac{P_t}{\eta_g} = \frac{142.7687kw}{0.95} \quad (3.8)$$

$$= 150.283KW$$

To propel the vehicle the motor drive can be select up to 168kW maximum power. This information is used to select the PMSM parameters.

Figure 3.4 illustrates the relationship between vehicle speed and the power required for propulsion. As vehicle speed increases, power consumption rises proportionally. The vehicle's maximum speed is achieved at a power consumption of 150kW. Accurate motor modeling necessitates determining both the rated and maximum torque requirements.

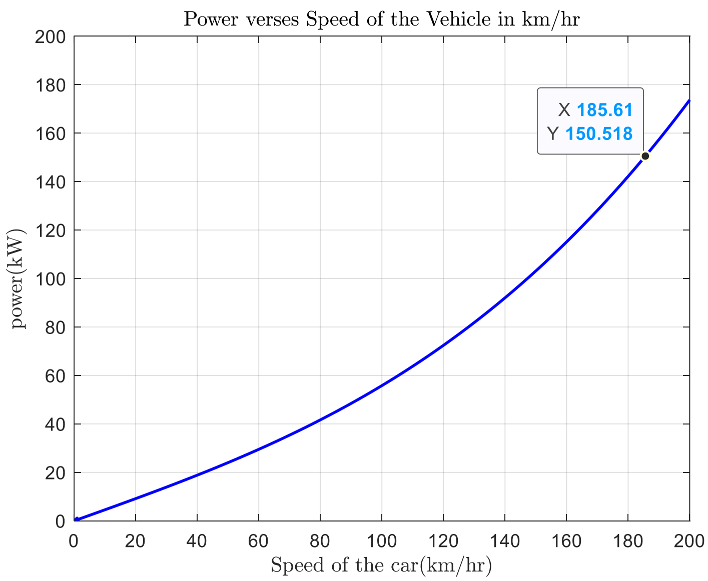

Figure 3.4 Relationship Between Driving Power and Vehicle Speed for the Hyundai Ioniq.

3.5.1.4 Required Torque at the Drive Wheel

Torque on the drive wheel calculation is necessary to calculate the vehicle's drive characteristics needed. Given an overall transmission efficiency of 89%, the actual torque load can be calculated as:

$$T_{load} = \frac{P_t}{\omega_m} \times \eta$$

$$= \frac{142.7687kw}{314} \times 0.89 \tag{3.9}$$

$$= 404.663Nm$$

Where, T_{load} is the actual torque rate, ω_m is rated speed of the motor from Table 3.3, and η is the transmission efficiency.

Table 3.3 IPMSM parameter specification (*Morimoto et al., 2006*).

parameter	symbol	value
Maximum power	P_m	168KW
Rated Power	P	125KW
Rated speed	ω_m	314 rad/s
Rated torque	T_e	412Nm
Stator resistance	R_s	0.01
d-axis Inductance	L_d	0.8mH
q-axis Inductance	L_q	1.6mH
Magnet flux	λ_m	0.17 Wb
Moment of inertia	J	0.015kg·m2
Viscous friction model	b	0.003Ns/m
Number of pole pairs	p	4

3.6 IPMSM Drive Modeling for Electric Vehicle Systems

For improving energy efficiency, extending battery life, and prolonging the life of electric vehicles such as the Hyundai Ioniq, accurate control of the motor speed is imperative since it has a direct effect on the overall vehicle performance and safety. One of the key parameters that affect vehicle safety is speed, which relies on the operation of the motor. Precise modeling of the electric motor, particularly the Interior Permanent Magnet Synchronous Motor (IPMSM), is fundamental in designing a good control system to propel the Hyundai Ioniq.

The stator and rotor are the two main components of the IPMSM. The stator is the stationary part and consists of three-phase windings sinusoidally distributed with 120° phase shift between phases. Permanent magnets are embedded in the rotor, which contributes numerous benefits like no brushes, no rotor losses, and lowering the motor's weight. These features make the IPMSM a prime candidate for the Hyundai Ioniq, offering increased torque density, efficiency, and reliability suitable for modern electric vehicle application.

3.6.1 Mathematical Modeling of IPMSM

A two-stage model of the Interior Permanent Magnet Synchronous Motor (IPMSM) in d-q coordinate form is employed for deriving the dynamic model. Through this method, the analysis is made easier by taking two stator windings and a single rotor magnet. The reference frame transformation is employed to transform the complex three-phase model into a reduced two-phase model.

3.6.1.1 Reference Frame Transformation

Reference frame transformations are crucial in electric machine control, particularly in interior permanent magnet synchronous motors, because they reduce the complexity of the mathematical representation and control design of the motor. Reference frame transformations convert time-varying three-phase variables into stationary or rotating reference frames, which enable torque and flux control decoupling in IPMSMs. This section provides a detailed description regarding reference frame transformations, their significance, and their application in the control of interior permanent magnet synchronous motors (IPMSMs).

Clark Transformation: The Clarke transformation converts a three-phase (abc) system into two components, α and β in a stationary orthogonal frame of reference. Two orthogonal axes, 90 degrees apart, are utilized by the clarke transformation to represent any space vector or phasor. The stator voltages of three-phase balanced voltages of a PMSM can be expressed as:

$$v_a = \sqrt{2}\, v_{rms} \sin(\omega t) \tag{3.10}$$

$$v_b = \sqrt{2}\, v_{rms} \sin\left(\omega t - \frac{2\pi}{3}\right) \tag{3.11}$$

$$v_c = \sqrt{2}\, v_{rms} \sin\left(\omega t + \frac{2\pi}{3}\right) \tag{3.12}$$

Figure 3.5 visually illustrates the Clark transformation, depicting the conversion from the three-phase system to the two-phase (αβ) system.

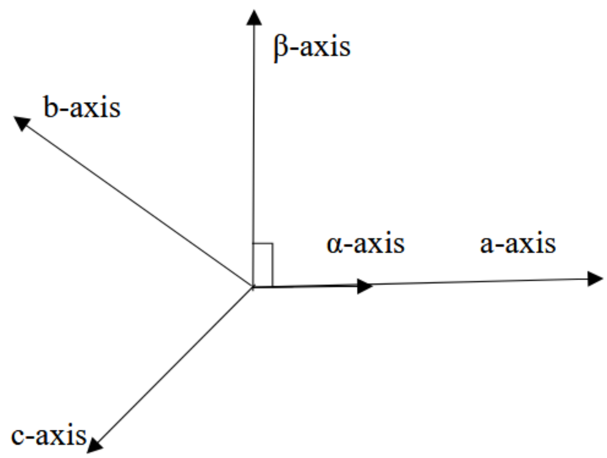

Figure 3.5 Clark transformation.

$$\begin{bmatrix} v_\alpha \\ v_\beta \\ v_0 \end{bmatrix} = \frac{2}{3} \begin{bmatrix} 1 & -\frac{1}{2} & -\frac{1}{2} \\ 0 & \frac{\sqrt{3}}{2} & -\frac{\sqrt{3}}{2} \\ \frac{1}{2} & \frac{1}{2} & \frac{1}{2} \end{bmatrix} \begin{bmatrix} v_a \\ v_b \\ v_c \end{bmatrix} \tag{3.13}$$

$$
\begin{bmatrix} v_a \\ v_b \\ v_c \end{bmatrix} = \frac{2}{3} \begin{bmatrix} 1 & 0 & 0 \\ -\frac{1}{2} & \frac{\sqrt{3}}{2} & 0 \\ -\frac{1}{2} & -\frac{\sqrt{3}}{2} & 0 \end{bmatrix} \begin{bmatrix} v_\alpha \\ v_\beta \\ v_0 \end{bmatrix} \tag{3.14}
$$

where V_a, V_b, and V_c represent the line voltages, a transformation to a two-phase system is often employed. the Clark transformation converts the three-phase voltages (Vabc) into two-phase components (Vαβ), and the inverse Clark transformation performs the reverse operation. These transformations are mathematically defined in Equations 3.13 and 3.14 respectively.

Park Transformation

The Park transformation converts the two components α and β derived via the Clarke transformation even more to a rotating orthogonal reference frame (dq). 'd' and 'q' are the direct and quadrature components, respectively, in this reference frame. Figure 3.6 illustrates this transformation, which shows the conversion of the αβ frame to the rotating d-q frame.

$$
\begin{bmatrix} v_d \\ v_q \end{bmatrix} = \begin{bmatrix} cos(\theta) & sin(\theta) \\ -sin(\theta) & cos(\theta) \end{bmatrix} \begin{bmatrix} v_\alpha \\ v_\beta \end{bmatrix} \tag{3.15}
$$

$$
\begin{bmatrix} v_\alpha \\ v_\beta \end{bmatrix} = \begin{bmatrix} cos(\theta) & -sin(\theta) \\ sin(\theta) & cos(\theta) \end{bmatrix} \begin{bmatrix} v_d \\ v_q \end{bmatrix} \tag{3.16}
$$

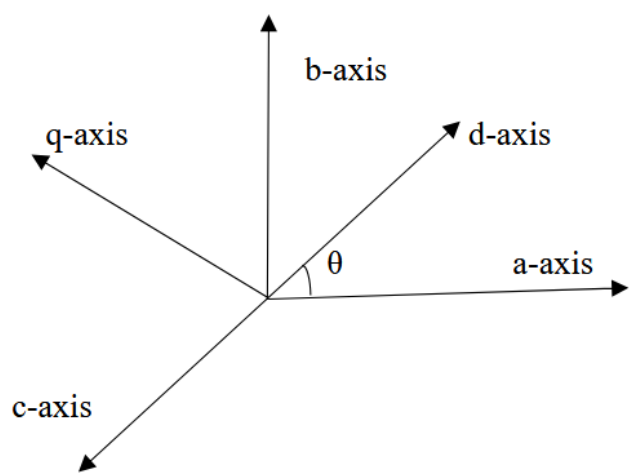

Figure 3.6 Park transformation.

3.6.2 Motor Model in dq Frame

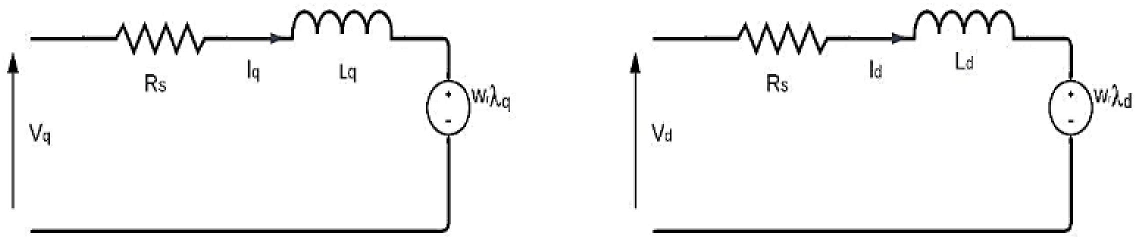

Figure 3.7 PMSM d-q axis equivalent circuit (Chai et al., 2013).

From Equations (3.13) and (3.15) the dq equivalent circuit can be derived to stator q-axis and d-axis as illustrated in Figure 3.7 (Chai et al., 2013).

$$v_d = R_s I_d + \frac{d}{dt}\lambda_d - \omega_r \lambda_q \tag{3.17}$$

$$v_q = R_s I_q + \frac{d}{dt}\lambda_q + \omega_r \lambda_d \tag{3.18}$$

Where, v_d is d-axis voltage and v_q is q-axis voltage, I_q is q-axis current and I_d is d-axis current λ_d is d-axis flux linkage and λ_q is q-axis flux linkage.

The d-q axis flux linkages are expressed by:

$$\lambda_d = L_d I_d + \lambda_m \tag{3.19}$$

$$\lambda_q = L_q I_q \tag{3.20}$$

Where, L_d is d-axis inductance and L_q is q-axis inductance λ_m is the permanent magnet flux linkage.

By substituting Equations (3.19) and (3.20) into Equations (3.17) and (3.18), the following results are obtained:

$$V_d = R_s I_d + \frac{d}{dt} L_d I_d - \omega_r L_q I_q \tag{3.21}$$

$$v_q = R_s I_q + \frac{d}{dt} L_q I_q + \omega_r (L_d I_d + \lambda_m) \tag{3.22}$$

The electromagnetic torque equation is expressed as:

$$T_e = \frac{3}{2}p(\lambda_m I_q + (L_d - L_q)I_d I_q) \quad (3.23)$$

And the mechanical torque equation is:

$$J\frac{d\omega_m}{dt} = T_e - b\omega_m - T_l \quad (3.24)$$

Where, T_e is electromagnetic torque, T_l is torque load, J is moment of inertia, b is the damping coefficient, and ω_m is mechanical speed.

Rearranging Equations (3.21) and (3.22) gives us:

$$\frac{d}{dt}I_d = -\frac{R_s}{L_d}I_d + \frac{\omega_r L_q I_q}{L_d} + \frac{V_d}{L_d} \quad (3.25)$$

$$\frac{d}{dt}I_q = -\frac{R_s}{L_q}I_q - \frac{\omega_r L_d I_d}{L_q} - \frac{\omega_r \lambda_m}{L_q} + \frac{v_q}{L_d} \quad (3.26)$$

Substituting Equation (3.24) into Equation (3.23) yields:

$$J\frac{d\omega_m}{dt} = \frac{3}{2}p(\lambda_m I_q + (L_d - L_q)I_d I_q) - b\omega_m - T_l \quad (3.27)$$

$$\frac{d\omega_m}{dt} = \frac{\frac{3}{2}p(\lambda_m I_q + (L_d - L_q)I_d I_q) - b\omega_m - T_l}{J} \quad (3.28)$$

3.6.2.1 State space model of IPMSM

To express Equations (3.25), (3.26) and (3.28) into state space:

Let $x_1 = I_d$, $x_2 = I_q$ and $x_3 = \omega_m$

$$\dot{x}_1 = \frac{V_d - R_s x_1 + L_q x_3 x_2}{L_d} \quad (3.29)$$

$$\dot{x}_2 = \frac{V_q - R_s x_2 - (L_d x_1 + \lambda_m)x_3}{L_q} \quad (3.30)$$

$$\dot{x}_3 = \frac{\frac{3}{2}p(\lambda_m x_2 + (L_d - L_q)x_1 x_2) - bx_3 - T_l}{J} \quad (3.31)$$

3.7 Voltage Source Inverters

Variable speed operation is possible only by variable frequency AC power supply by IPMSM motors. As most of the vehicles employ DC batteries, a power electronic converter has to be employed, which requires the employment of a three-phase voltage source inverter. With six gate signals produced by SVPWM, semiconductor switches of such an inverter are controlled in order to generate the necessary variable frequency AC voltage (Colak et al., 2011).

Figure 3.8 shows a diagram displaying this three phase VSI (Boby, 2013).

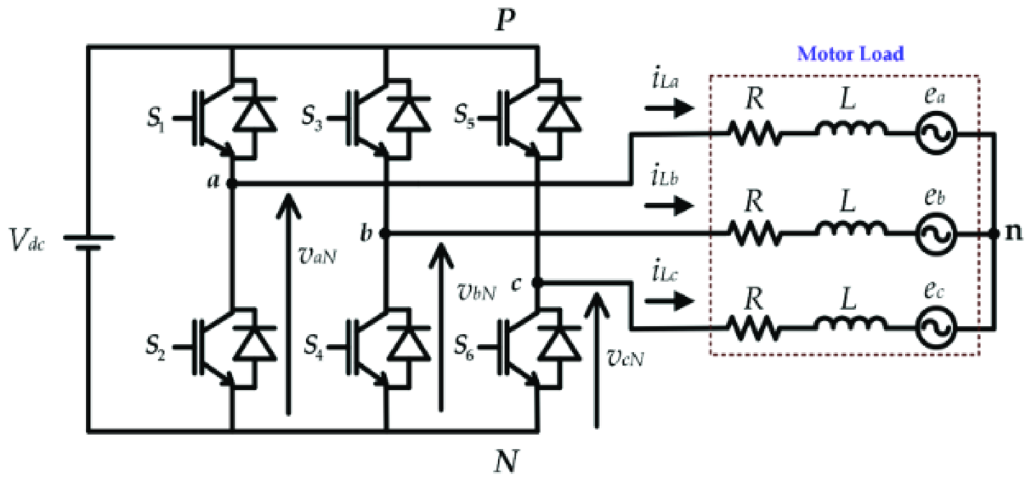

Figure 3.8 Three phase inverter.

3.8 Space Vector Pulse Width Modulation (SVPWM)

A complex way of generating PWM signals in three phase inverters is known as space vector modulation. Compared to traditional PWM methods, SVM offers improved performance by offering output voltages with more fundamental content and reduced harmonic distortion. The fundamental goal of all modulation methods is to give an output voltage of varying shape with low harmonic distortion as the optimum, and SVM is optimum to serve this function for variable frequency drive applications (Liang et al., 2014).

Determining sectors

As shown in Figure 3.9, a reference voltage (V_{ref}) located in sector 1 has an angle (θ) between 0 and 60 degrees. Due to its rotational movement, determined by the inverter's frequency, the reference voltage can be positioned in any of the six sectors.

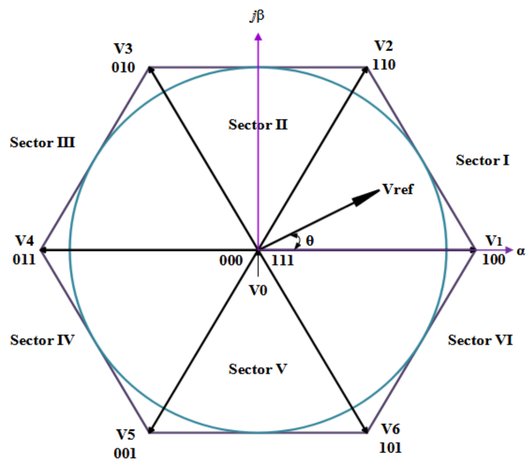

Figure 3.9 Diagram of Space Vectors for a Two-Level Inverter (Dong et al.,2018).

Switching States

The output voltage vectors corresponding to switching states are listed below (Kumar et al., 2010).

Table 3.4 Inverter Switching States and Output Vectors.

Voltage vector	Switching vector			Line to neutral Voltage			Line to line voltage		
	a	b	c	V_{an}	V_{bn}	V_{cn}	V_{ab}	V_{bc}	V_{ac}
V0	0	0	0	0	0	0	0	0	0
V1	1	0	0	2/3	-1/3	-1/3	1	0	-1
V2	1	1	0	1/3	1/3	-2/3	0	1	-1
V3	0	1	0	-1/3	2/3	-1/3	-1	1	0
V4	0	1	1	-2/3	1/3	1/3	-1	0	1
V5	0	0	1	-1/3	-1/3	2/3	0	-1	1
V6	1	0	1	1/3	-2/3	1/3	1	-1	0
V7	1	1	1	0	0	0	1	0	0

Procedure implement SVPWM

Space Vector PWM implementation involves the following steps:

1. **Determine reference values**: Calculate V_q, V_d, V_{ref}, and the angle of a sector (α).

2. **Calculate duty cycles**: Based on the sector and reference vector, calculate the times T0, T1, and T2.
3. **Determine switching times**: Calculate the exact switching instants for each transistor (S1 to S6) based on the calculated duty cycles.

Step-1: Calculate angle(α), V_α, V_β, and V_{ref}.

The α-β frame is used by SVPWM and the Clarke transformation is applied, as opposed to the a-b- c reference frame. Hence, V_α and V_β are supplied as input to SVPWM. This voltage was calculated using the formula below:

$$\begin{bmatrix} v_\alpha \\ v_\beta \end{bmatrix} = \frac{2}{3} \begin{bmatrix} 1 & -\frac{1}{2} & -\frac{1}{2} \\ 0 & \frac{\sqrt{3}}{2} & -\frac{\sqrt{3}}{2} \end{bmatrix} \begin{bmatrix} v_{an} \\ v_{bn} \\ v_{cn} \end{bmatrix} \tag{3.32}$$

We can quickly ascertain the reference voltage (V_{ref}) and angle α as follows after determining V_α and V_β.

$$\begin{gathered} \left| v_{ref} \right| = \sqrt{v_\alpha^{\ 2} + v_\beta^{\ 2}} \\ \alpha = \tan^{-1}\left(\frac{v_\beta}{v_\alpha} \right) \end{gathered} \tag{3.33}$$

Step 2: Determine how long T1, T2, and T0 will last. The inverter switches' on-time lengths are represented by the time intervals T1, T2, and T0. These timings can be calculated for Sector 1 as follows:

$$\begin{gathered} \int_0^{ts} v_{ref} = \int_0^{T1} V_1 \mathrm{d}t + \int_{T1}^{T1+T2} V_2 \mathrm{d}t + \int_{T1+T2}^{TS} V_0 \\ Ts\ v_{ref} . \begin{bmatrix} \cos(\alpha) \\ \sin(\alpha) \end{bmatrix} = T1 . \frac{2}{3} . V_{dc} . \begin{bmatrix} 1 \\ 0 \end{bmatrix} + T2 . \frac{2}{3} . V_{dc} . \begin{bmatrix} \cos\left(\frac{\pi}{3}\right) \\ \sin\left(\frac{\pi}{3}\right) \end{bmatrix} \end{gathered} \tag{3.34}$$

$$T2 = Ts.\alpha.\frac{\sin(\alpha)}{\sin\left(\frac{\pi}{3}\right)} \tag{3.35}$$

where Ts and α are total switching time and modulation index which are presented in following Equations:

$$Ts = \frac{1}{f_s} \; and \; a = \frac{\left|v_{ref}\right|}{\frac{2}{3}.v_{dc}} \tag{3.36}$$

$$T1 = \frac{\sqrt{3}.T_z.\left|v_{ref}\right|}{V_{dc}}.\sin\left(\frac{n}{3}\pi - \alpha\right) \tag{3.37}$$

$$T2 = \frac{\sqrt{3}.T_z.\left|V_{ref}\right|}{V_{dc}}.\left(\sin\left(\alpha - \frac{n-1}{3}\pi\right)\right)$$

Step 3: Find out when each transistor switches on and off.

The bottom switch of the inverter is off while the equivalent upper switch is on, and vice versa. This is how the switches work together complimentary. The specific switching times for each transistor within a given sector is detailed in the Table 3.5 (Kumar et al., 2010):

Table 3.5 Calculating the switching time in every sector.

Sector number (n)	Upper Switches (S_1, S_3, S_5)	Lower Switches (S_2, S_4 S_6)
1	$S_1=T_1+T_2+T_0/2$ $S_3=T_2+T_0/2$ $S_5=T_0/2$	$S_4=T_0/2$ $S_6=T_1+T_0/2$ $S_2=T_1+T_2+T_0/2$
2	$S_1=T_1+T_0/2$ $S_3=T_1+T_2+T_0/2$ $S_5=T_0/2$	$S_4= T_2+T_0/2$ $S_6=T_0/2$ $S_2=T_1+T_2+T_0/2$
3	$S_1= T_0/2$ $S_3=T_1+T_2+T_0/2$ $S_5=T_2+T_0/2$	$S_4= T_1+T_2+T_0/2$ $S_6=T_2+T_0/2$ $S_2=T_0/2$
4	$S_1= T_0/2$ $S_3=T_1+T_0/2$ $S_5= T_1+T_2+T_0/2$	$S_4= T_1+T_2+T_0/2$ $S_6=T_2+T_0/2$ $S_2= T_0/2$
5	$S_1=T_2+T_0/2$ $S_3=T_0/2$ $S_5= T_1+T_2+T_0/2$	$S_4= T_1+T_0/2$ $S_6=T_1+ T_2+T_0/2$ $S_2=T_0/2$
6	$S_1=T_1+T_2+T_0/2$ $S_2=T_0/2$ $S_3=T_1+T_0/2$	$S_1= T_0/2$ $S_2= T_1+T_2+T_0/2$ $S_3=T_2+T_0/2$

CHAPTER FOUR

CONTROLLER DESIGN

4.1 Design of a Nonlinear Model Predictive Speed Controller

Nonlinear Model Predictive Controller (NMPC) is a control strategy that is particularly well-suited for systems with nonlinear dynamics. Compared to linear model predictive control, NMPC is not founded on linear approximations and hence can treat advanced system behavior more appropriately.

In MPC there are three strategies:

- Prediction: - to know how the state evolves.
- Online optimization: -by minimizing the difference between prediction and reference then by manipulating the control action.
- Receding horizon implementation: -we do this every sampling time or every time step.

The NMPC optimizes a control sequence over a finite prediction horizon at each sampling instant. This involves the solving of an optimization problem to compute the optimal control inputs that would drive the given cost function to its minimum possible value under the system constraints. The first control action in the optimized sequence is then applied to the system and the cycle repeats at the subsequent sampling instant.

The used cost function for the optimization both penalized the difference between system state and setpoint, as well as control input size. Penalizing the control input has the algorithm attempt to conserve energy and minimize usage of excessive control effort. The outcome is a control policy that is energy efficient and saves energy (Grüne et al., 2011). The well-known type of cost function satisfying the above condition is given by:

$$l(x,u) = (x - x_*)^T Q (x - x_*) + (u - u_*)^T R (u - u_*) \tag{4.1}$$

where Q is the state weight matrix, which is used to penalize the error between the actual state and the reference value, and R is the control weight matrix, which is used to penalize the control input.

By using Δu in the cost function we can Improve the smoothness of applied input currents i_d and i_q, that means it controls the current i_d and i_q to not change aggressively.

So, the cost function becomes;

$$l(x,u) = (x - x_*)^T Q (x - x_*) + (u - u_*)^T R_1 (u - u_*) + (\triangle u)^T R_2 (\triangle u) \tag{4.2}$$

where R_1 is input control weight matrix and R_2 change in input control weight matrix and $\triangle u = u(k) - u(k-1)$.

In this research, NMPC is used for speed controls as outer loop controller. This controller gives reference currents for internal PI current controllers.

Therefore, the states and the control variables of this NMPC are:

$$x_1 = u_1, x_2 = u_2, x_3 = x, T_l = d = u_3$$

From the developed dynamic Equations, the state space representation of speed is:

$$\dot{x}_3 = \frac{\frac{3}{2} p(\lambda_m x_2 + (L_d - L_q) x_1 x_2) - b x_3 - T_l}{J} \tag{4.3}$$

Substituting the defined states and control variables in the above Equation gives us:

$$\dot{x} = \frac{\frac{3}{2} p(\lambda_m u_2 + (L_d - L_q) u_1 u_2) - b x - T_l}{J} \tag{4.4}$$

The dynamic mode for NMPC controller is given by:

$$\dot{x} = f_c(x(t)), u(t)) \tag{4.5}$$

In order to change this continuous time model to discrete time Euler discretization method is used.

$$x(k+1) = f(x(k)), u(k)) \tag{4.6}$$

Optimal control problem looks like:

$$\underset{u}{\text{Minimize}}\; J_N(x_0, u) = \sum_{k=0}^{N-1} l(x_u(k), u(k), (\triangle u)) \tag{4.7a}$$

$$\text{Subject to: } x_u(k+1) = f(x_u(k), u(k)), \tag{4.7b}$$

$$u(k) \in U, \forall k \in [0, N-1] \tag{4.7c}$$

$$x_u(k) \in X, \forall k \in [0,N] \tag{4.7d}$$

The standard problem formulation in numerical optimization is called Nonlinear Programming Problem (NLP) and it has a general form as follows:

$$\text{Min } \phi(w) \qquad \text{objective function}$$

$$\text{s.t. } g_1(w) \leq 0, \qquad \text{inequality constraints}$$

$$g_2(w) = 0, \qquad \text{equality constraints}$$

To discretize or convert the Optimal Control Problem (OCP) to nonlinear programming problem (NLP) we can use different techniques like single shooting, multiple shooting and collocation method but for this thesis among these three techniques single shooting is used for simplicity.

Single shooting: is a direct optimization technique used within Nonlinear Model Predictive Control (NMPC). The approach transforms the control problem into an NLP problem by discretization of the control inputs over the prediction horizon and solving the forward-in-time system dynamics with such control inputs. Contrary to multiple shooting, where the horizon is partitioned into segments and the intermediate states are solved for, single shooting combines system dynamics from a single initial state and only optimizes the control variables. It is computationally effective.

To predict future states in research Runge-Kutta 4^{th}-order approach is used and it's Equation is described by:

$$x(k+1) = x(k) + \frac{h}{6}(k_1 + 2k_2 + 2k_3 + k_4) \tag{4.8}$$

Where ,

$$k_1 = hf(k, x(k), u(k)), k_2 = hf(k + \frac{h}{2}, x(k) + \frac{k_1}{2}, u(k)),$$

$$k_3 = hf(k + \frac{h}{2}, x(k) + \frac{k_2}{2}, u(k)), k_4 = hf(k + h, x(k) + k_3, u(k))$$

Constraints

What makes NMPC successful is that it can directly handle constraints. In thesis constraint is applied on the control variables, i_D and i_Q

The upper boundaries of the currents are set to be their nominal values and lower boundaries will be negative of the maximum nominal values. i.e.

$$-i_{Ds-nom} \le i_{Ds} \le i_{Ds-nom} \text{ and } -i_{Qs-nom} \le i_{Qs} \le i_{Qs-nom} \tag{4.9}$$

4.2 PI Current Controller

The outer loop controller determines the reference stator current values required to achieve the requested speed. It takes input speed commands and decides on the respective stator current references required to meet these demands. These current references are used for regulation of the supply voltage fed to the stator.

For precise control, PI controllers are employed to control the reference voltage levels based on the computed current references. Two internal PI current regulators are incorporated in the control system namely one for d-axis current and the other for q-axis current so that there is satisfactory current regulation for smooth and efficient motor running.

The outer loop controller gives current references as:

$$i*_Q \text{ and } i*_D$$

The errors between the references and stator currents are described as below.

$$e_D = i*_D - i_D \tag{4.10}$$

$$e_Q = i*_Q - i_Q \tag{4.11}$$

Let the PI controller gains be K_{p1}, K_{i1}, K_{P2},K_{i2}

The D- and Q-axis voltage references are calculated as:

$$v^*_D = K_{P2} e_D + K_{i2} \int e_D dt \tag{4.12}$$

$$v^*_Q = K_{P1} e_Q + K_{i1} \int e_Q dt \tag{4.13}$$

4.2.1 Genetic Algorithm for PI Tuning

Genetic Algorithm (GA) is used to optimize and based on a fitness function that minimizes current tracking error and improves system stability. The GA optimization follows these steps:

1. **Initialization**: Generate a population of random values.
2. **Fitness Evaluation**: Compute a cost function based on the integral of absolute error (IAE).
3. **Selection, Crossover, Mutation**: Apply genetic operations to evolve parameters.
4. **Convergence**: Repeat until optimal parameters are found.

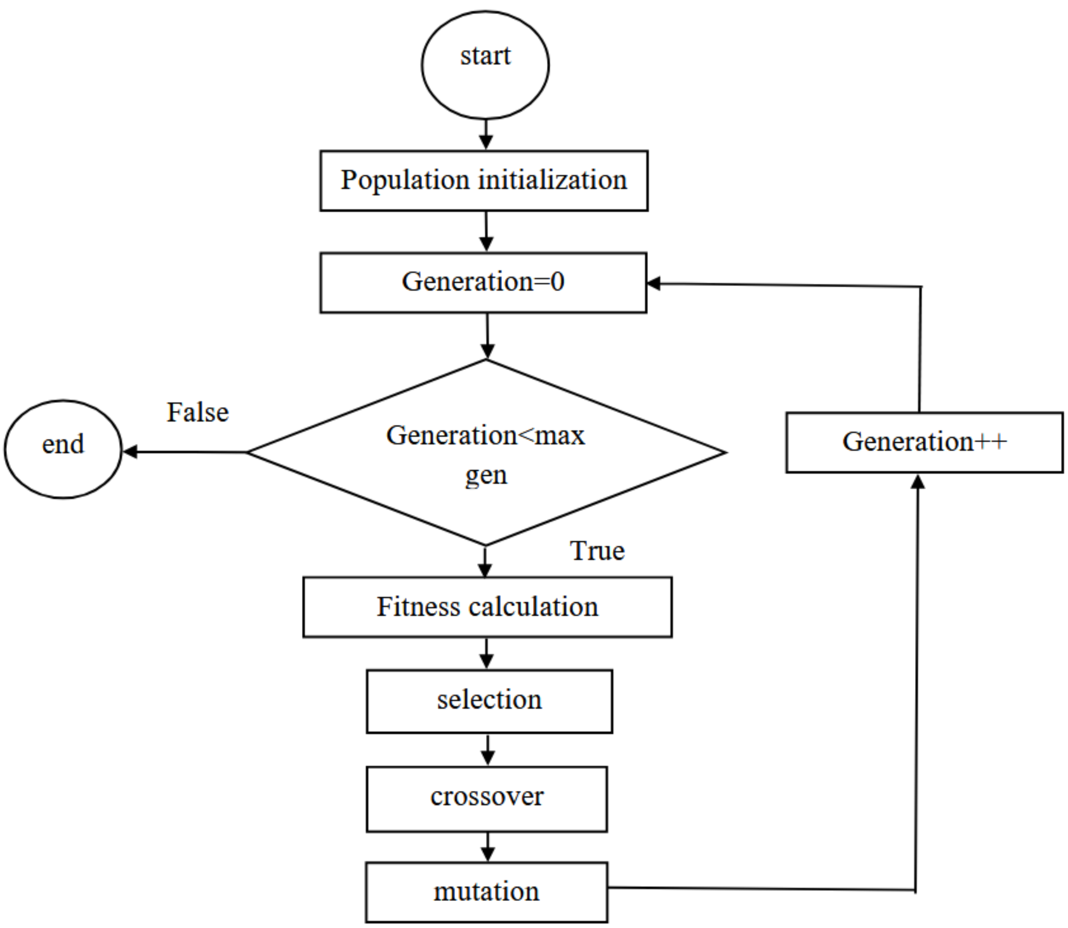

Figure 4.1 Flow chart of genetic algorithm optimization (Oubelaid et al.,2022).

Performance Index in GA Tuning

The Integral of Absolute Error (IAE) was used as the performance index (cost function) in the GA-based optimization.

The IAE is defined as:

$$IAE = \int_0^T |e(t)|\, dt \tag{4.14}$$

Where e(t) is the tracking error between the reference current or speed and the actual current or speed, respectively, depending on the control loop. It was selected as the measure because it rightfully penalizes overall tracking errors accumulated with time to give more precise steady-state and smoother responses.

The GA optimization was performed by invoking MATLAB's inbuilt function ga () to run the objective function that computed the IAE with regard to the closed-loop system response. The PI gains (K_{p1}, K_{i1}, K_{p2}, K_{i2}) were tuned for minimizing the IAE value of the given reference tracking problem.

The graphical result of the optimized object function (IAE) parameter of the cascade control system is shown below in Figure 4.2 Its value after many times re-optimization is 1.03208.

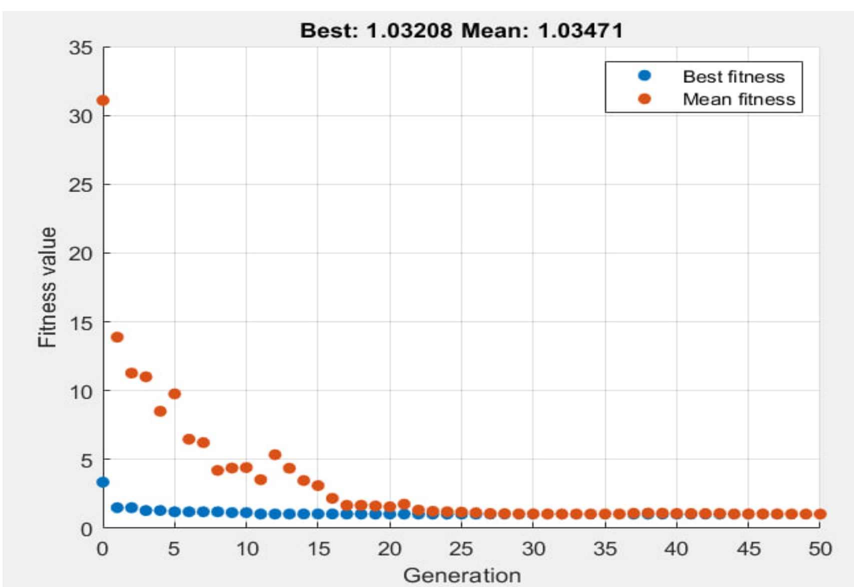

Figure 4.2 Fitness values vs generation for object function

4.3 Linear Model Predictive Speed Controller

This work employs a Linear Model Predictive Controller (LMPC) as an outer loop replacement for speed control. LMPC and Nonlinear Model Predictive Control (NMPC) are compared.

Linear Model Predictive Controller, is a discrete-time model predictive control method. It does optimization of a cost function by manipulating control increments. Thus, the description of the continuous-time system must be discretized for implementation.

The first process step towards application of LMPC is to linearize the nonlinear state equation (model) given in the form of Equation (4.4). Linear approximation with a linear model constructed around measured states does the linearization. The states considered in this process are:

$x = \omega_m$, $u_1 = i_q$, $u_2 = i_d$, and $d = T_l$

Let the equilibrium points be x^*, u^*, y^*

Then the errors between instant and equilibrium points are:

$\bar{x} = x - x^*, \bar{u} = u - u^*, \bar{y} = y - y^*$

Hence, the instant vectors are

$$x = \bar{x} + x^*, u = \bar{u} + u^*, y = \bar{y} + y^* \tag{4.15}$$

The state and output Equations in nonlinear model are given as:

$$\dot{x} = f(x,u) \text{ and } y = g(x,u) \tag{4.16}$$

Substituting Equation (4.15) into Equation (4.16) yields:

$$\dot{\bar{x}} + \dot{x}^* = f(\bar{x} + x^*, \bar{u} + u^*) \tag{4.17}$$

$$\bar{y} + y^* = g(\bar{x} + x^*, \bar{u} + u^*) \tag{4.18}$$

Using the Tylor series,

$$\dot{\bar{x}} + \dot{x}^* = f(x^*, u^*) + \bar{x} \left.\frac{\partial f}{\partial x}\right|_{\substack{x = x^* \\ u = u^*}} + \bar{u} \left.\frac{\partial f}{\partial u}\right|_{\substack{x = x^* \\ u = u^*}} \tag{4.19}$$

$$\bar{y} + y^* = g(\bar{x}, \bar{u}) + \bar{x} \left.\frac{\partial g}{\partial x}\right|_{\substack{x = x^* \\ u = u^*}} + \bar{u} \left.\frac{\partial g}{\partial u}\right|_{\substack{x = x^* \\ u = u^*}} \tag{4.20}$$

But at equilibrium points,

$$\dot{x}^* = f(x^*, u^*) \tag{4.21}$$

$$y^* = g(x^*, u^*) \tag{4.22}$$

Hence, Equations (4.19) and (4.20) are determined to be:

$$\dot{\bar{x}} = \bar{x} \left.\frac{\partial f}{\partial x}\right|_{\substack{x = x^* \\ u = u^*}} + \bar{u} \left.\frac{\partial f}{\partial u}\right|_{\substack{x = x^* \\ u = u^*}} \tag{4.23}$$

$$\bar{y} = \bar{x} \left.\frac{\partial g}{\partial x}\right|_{\substack{x = x^* \\ u = u^*}} + \bar{u} \left.\frac{\partial g}{\partial u}\right|_{\substack{x = x^* \\ u = u^*}} \tag{4.24}$$

Let $A = \left.\frac{\partial f}{\partial x}\right|_{\substack{x = x^* \\ u = u^*}}$, $B = \left.\frac{\partial f}{\partial u}\right|_{\substack{x = x^* \\ u = u^*}}$, $C = \left.\frac{\partial g}{\partial x}\right|_{\substack{x = x^* \\ u = u^*}}$ and $D = \left.\frac{\partial g}{\partial u}\right|_{\substack{x = x^* \\ u = u^*}}$

In general, Equations (4.23) and (4.24) are expressed as:

$$\dot{\bar{x}} = A\bar{x} + B\bar{u} \tag{4.25}$$

$$\bar{y} = C\bar{x} + D\bar{u} \tag{4.26}$$

Equations (4.25) and (4.26) are linearized state and output equations of the system.

The nonlinear dynamic model functions *f* and *g* are defined as:

$$f = \frac{\frac{3}{2}p(\lambda_m x_2 + (L_d - L_q)x_1 x_2) - bx_3 - T_l}{J}, g = x \tag{4.27}$$

The Equations (4.25) and (4.26) are in continuous time so they have to be converted to discrete time and use step size $T_s = 0.005s$.

$$x(k+1) = A_d x(k) + B_d u(k) + d_\varepsilon \tag{4.28}$$

$$y(k) = C_d x(k) \tag{4.29}$$

The new state variable vector is defined as:

$$X(k) = [\,\triangle x(k) \quad y(k)\,]^T \tag{4.30}$$

Based on the construction of the augmented state space model, the next step in the design of predictive control system is to compute the predicted plant output using the future control action.

The prediction is formulated within an optimization horizon. Let the current time be k and the state variable be measurable at this time. Then the future state variable and the future control path are given by:

$$X(k+1|k),\ X(k+2|k),\ X(k+3|k),\ \dots\ X(k+N_P|k)$$

$$\Delta u(k), \Delta u(k+1), \Delta u(k+2),\ \dots \Delta u(k+N_c)$$

Where, H_p is prediction horizon which is the length of the optimization window, H_c is control horizon which gives the parameters used to capture the future control signal. Then the future state variable can be calculated as follows:

$$X(k+1|k) = AX(k) + B\Delta u(k)$$

$$X(k+2|k) = AX(k+1|k) + B\Delta u(k+1) = A^2X(k) + \sum_{i=0}^{2-1} A^{2-i-1}B\Delta u(k+i)$$

$$\vdots \tag{4.31}$$

$$X\left(k+H_p|k\right) = AX\left(k+H_p|k\right) + B\Delta u\left(k+H_p\right) = A^{H_p}X(k) + \sum_{i=0}^{H_p-1} A^{H_p-i-1}B\Delta u(k+i) \quad if\ H_p \geq H_c$$

$$X\left(k+H_p|k\right) = AX\left(k+H_p|k\right) + B\Delta u\left(k+H_p\right) = A^{H_p}X(k) + \sum_{i=0}^{Hc-1} A^{H_p-i-1}B\Delta u(k+i) \quad if\ H_p < H_c$$

From the predicted state variables, the predictive output variables are:

$$
\begin{aligned}
y(k+1|k) &= CX(k+1|k) = CAX(k) + CB\Delta u(k) \\
y(k+2|k) &= CX(k+2|k) = CA^2X(k) + \sum_{i=0}^{2-1} CA^{2-i-1}B\Delta u(k+i) \\
&\;\;\vdots \\
y\left(k+H_p|k\right) &= CX(k+3|k) = CA^{H_p}X(k) + \sum_{i=0}^{H_p-1} CA^{H_p-i-1}B\Delta u(k+i) \;\; if\ H_p = H_c \\
y\left(k+H_p|k\right) &= CX(k+3|k) = CA^{H_p}X(k) + \sum_{i=0}^{H_c-1} CA^{H_p-i-1}B\Delta u(k+i) \;\; if\ H_p > H_c
\end{aligned}
\tag{4.32}
$$

The predictive output variable is expressed by present time state variable X(k) and future control variables. Equation (4.32) can be transformed into matrix form as follows:

$$
Y = EX(k) + Q\Delta U \tag{4.33}
$$

Where, $E = \begin{bmatrix} CA \\ CA^2 \\ \vdots \\ CA^{N_p} \end{bmatrix}$, $\mathrm{Q} = \begin{bmatrix} CB & 0 & \cdots & 0 \\ CAB & CB & \cdots & 0 \\ \vdots & \vdots & \ddots & \vdots \\ CA^{N_P-1}B & CA^{N_P-2}B & \cdots & CA^{N_P-N_C}B \end{bmatrix}$

In optimal control, the optimization is considered in reducing the error between the set point value and the predicted state output. Since the final value is defined, the optimization is done as a fixed final state optimization. It can be written as:

$$
J = \frac{1}{2}\int_0^{\infty}((R_s - Y)^TQ(R_s - Y) + \Delta U^TR\Delta U)dt \tag{4.34}
$$

where, R_s is the desired speed (set point). Q and R are the weighting matrices of the output errors and input increments.

The predicted input signals for three consecutive time steps can be expressed as:

$$u(k) = u(k-1) + \Delta u(k)$$
$$u(k+1) = u(k) + \Delta u(k+1) = u(k-1) + \Delta u(k) + \Delta u(k+1)$$
$$u(k+2) = u(k+1) + \Delta u(k+2) = u(k-1) + \Delta u(k) + \Delta u(k+1) + \Delta u(k+2)$$

The future control value at any time-step n before the end of the control horizon is calculated as:

$$u(k+n) = u(k+n-1) + \Delta u(k+n) = u(k-1) + \sum_{i=0}^{n} \Delta u(k+i)$$

The constraints for the sequence of future control increments, ΔU, are summarized below. The coefficient matrix that multiplies these increments consists of identity matrices, *I*. These matrices are 2×2, reflecting the two control signals.

$$\begin{bmatrix} I & 0 & \cdots & 0 \\ I & I & \cdots & 0 \\ \vdots & \vdots & \ddots & \vdots \\ I & I & \cdots & I \end{bmatrix} \begin{bmatrix} \Delta u(k) \\ \Delta u(k+1) \\ \vdots \\ \Delta u(k+N_c-1) \end{bmatrix} \leq \begin{bmatrix} u_{\max} - u(k-1) \\ u_{\max} - u(k-1) \\ \vdots \\ u_{\max} - u(k-1) \end{bmatrix}$$
$$\begin{bmatrix} -I & 0 & \cdots & 0 \\ -I & -I & \cdots & 0 \\ \vdots & \vdots & \ddots & \vdots \\ -I & -I & \cdots & -I \end{bmatrix} \begin{bmatrix} \Delta u(k) \\ \Delta u(k+1) \\ \vdots \\ \Delta u(k+N_c-1) \end{bmatrix} \leq \begin{bmatrix} -u_{\min} + u(k-1) \\ -u_{\min} + u(k-1) \\ \vdots \\ -u_{\min} + u(k-1) \end{bmatrix}$$

It can be written as a compact form as follows:

$$M_1 * \triangle U \leq N_1 \tag{4.35}$$

where, $M_1 = \begin{bmatrix} I & 0 & \cdots & 0 \\ I & I & \cdots & 0 \\ \vdots & \vdots & \ddots & \vdots \\ I & I & \cdots & I \\ -I & 0 & \cdots & 0 \\ -I & -I & \cdots & 0 \\ \vdots & \vdots & \ddots & \vdots \\ -I & -I & \cdots & -I \end{bmatrix}$, $N_1 = \begin{bmatrix} u_{\max} - u(k-1) \\ u_{\max} - u(k-1) \\ \vdots \\ u_{\max} - u(k-1) \\ -u_{\min} + u(k-1) \\ -u_{\min} + u(k-1) \\ \vdots \\ -u_{\min} + u(k-1) \end{bmatrix}$

Δu, the increment of the input signal, is limited to the range between Δu_{min} and Δu_{max}. The following describes the constraints on an arbitrary increment.

$$\Delta u_{\min} \le \Delta u(k+n) \le \Delta u_{\max}$$

When we write the expression it becomes:

$$\begin{bmatrix} I & 0 & \cdots & 0 \\ 0 & I & \cdots & 0 \\ \vdots & \vdots & \ddots & \vdots \\ 0 & 0 & \cdots & I \end{bmatrix} \begin{bmatrix} \Delta u(k) \\ \Delta u(k+1) \\ \vdots \\ \Delta u(k+N_c-1) \end{bmatrix} \le \begin{bmatrix} \Delta u_{\max} \\ \Delta u_{\max} \\ \vdots \\ \Delta u_{\max} \end{bmatrix}$$

$$\begin{bmatrix} -I & 0 & \cdots & 0 \\ -I & -I & \cdots & 0 \\ \vdots & \vdots & \ddots & \vdots \\ -I & -I & \cdots & -I \end{bmatrix} \begin{bmatrix} \Delta u(k) \\ \Delta u(k+1) \\ \vdots \\ \Delta u(k+N_c-1) \end{bmatrix} \le \begin{bmatrix} -\Delta u_{\min} \\ -\Delta u_{\min} \\ \vdots \\ -\Delta u_{\min} \end{bmatrix}$$

In compact form we can write as:

$$M_2 * \triangle U \le N_2 \tag{4.36}$$

where, $M_2 = \begin{bmatrix} I & 0 & \cdots & 0 \\ 0 & I & \cdots & 0 \\ \vdots & \vdots & \ddots & \vdots \\ 0 & 0 & \cdots & I \\ -I & 0 & \cdots & 0 \\ -I & -I & \cdots & 0 \\ \vdots & \vdots & \ddots & \vdots \\ -I & -I & \cdots & -I \end{bmatrix}$, $N_2 = \begin{bmatrix} \Delta u_{\max} \\ \Delta u_{\max} \\ \vdots \\ \Delta u_{\max} \\ -\Delta u_{\min} \\ -\Delta u_{\min} \\ \vdots \\ -\Delta u_{\min} \end{bmatrix}$

For the output the Equation becomes:

$$\begin{aligned} & Y_{\min} \le Ez(k) + F\Delta U \le Y_{\max} \\ & Y_{\min} - Ez(k) \le F\Delta U \le Y_{\max} - Ez(k) \\ & -F\Delta U \le -Y_{\min} + Ez(k) \ , \ F\Delta U \le Y_{\max} - Ez(k) \end{aligned}$$

In compact form:

$$M_3 * \triangle U \leq N_3 \tag{4.37}$$

where, $M_3 = \begin{bmatrix} -F \\ F \end{bmatrix}$, $N_3 = \begin{bmatrix} -Y_{\min} + Ez(k) \\ Y_{\max} - Ez(k) \end{bmatrix}$

According to Equation above the final optimization problem is:

$$\begin{aligned} &\min_{\Delta U} J = \frac{1}{2}\left((R_s - Y)^T Q (R_s - Y) + \Delta U^T R \Delta U\right) \\ &\textit{such that } M * \Delta U \leq N \end{aligned} \tag{4.38}$$

where, $M = \begin{bmatrix} M_1 \\ M_2 \\ M_3 \end{bmatrix}$, $N = \begin{bmatrix} N_1 \\ N_2 \\ N_3 \end{bmatrix}$

CHAPTER FIVE

SIMULATION RESULT AND DISCUSSION

This chapter shows the results and analysis of simulation for the proposed speed control method using an Interior Permanent Magnet Synchronous Motor (IPMSM) in an electric vehicle (Hyundai Ioniq). According to motor parameters provided in Table 3.3, the performance of Nonlinear Model Predictive Control (NMPC) for speed control is examined. The current control that is associated with it is handled by a PI controller, and its gains are tuned with an optimization using a Genetic Algorithm (GA). A comparison is also provided between the NMPC and a Linear MPC (LMPC) solution based on identical motor parameters and working conditions to analyze the efficacy of each of the control strategies.

5.1 Performance of NMPC

In this section the system performance of Non-Linear Model predictive control (NMPC) is simulated and discussed for IPMSM.

The constraint applied on the current references (Inputs) are:

$$i_{q\ ref\_min} = -100,\ i_{q\ ref\_max} = 350,\ i_{d\ ref\_min} = -200,\ i_{d\ ref\_max} = 0$$

Np=10 is used for prediction horizon and the weighting matrix for the cost function are as follows:

Q:-penalizes speed tracking error.

Since the system has only one state, the weighting matrix Q is a scalar and is set to 1.

R_1:-penalizes magnitude of the control input(currents)to reduce power loss or overheating.

$$R_1 = \begin{bmatrix} 0.1 & 0 \\ 0 & 0.1 \end{bmatrix}$$

R_2:-penalizes the control input increments to ensure smoothness and avoid control chattering.

$$R_2 = \begin{bmatrix} 0.1 & 0 \\ 0 & 0.1 \end{bmatrix}$$

For PI current control, the gains are obtained by GA tuning algorithm.

The proportional term of the PI controller provides a control action proportional to the current error (K_{p1}, K_{p2}). K_{p1} and K_{p2} are for the i_q and i_d proportional current loop gain, respectively.

The integral term of the PI controller helps to eliminate steady-state errors by accumulating the past errors (K_{i1}, K_{i2}). K_{i1} is proportional gain for the i_q current loop and K_{i2} is proportional gain for i_d current loop.

	Proportional gain	Integral gain
i_q Current loop gain	0.2438	2.9024
i_d Current loop gain	0.0248	6.5563

Figure 5.1, shows the closed-loop response of NMPC with PI as inner current controller. It followed the reference speed (314 rad/sec) within a short time and high performance.

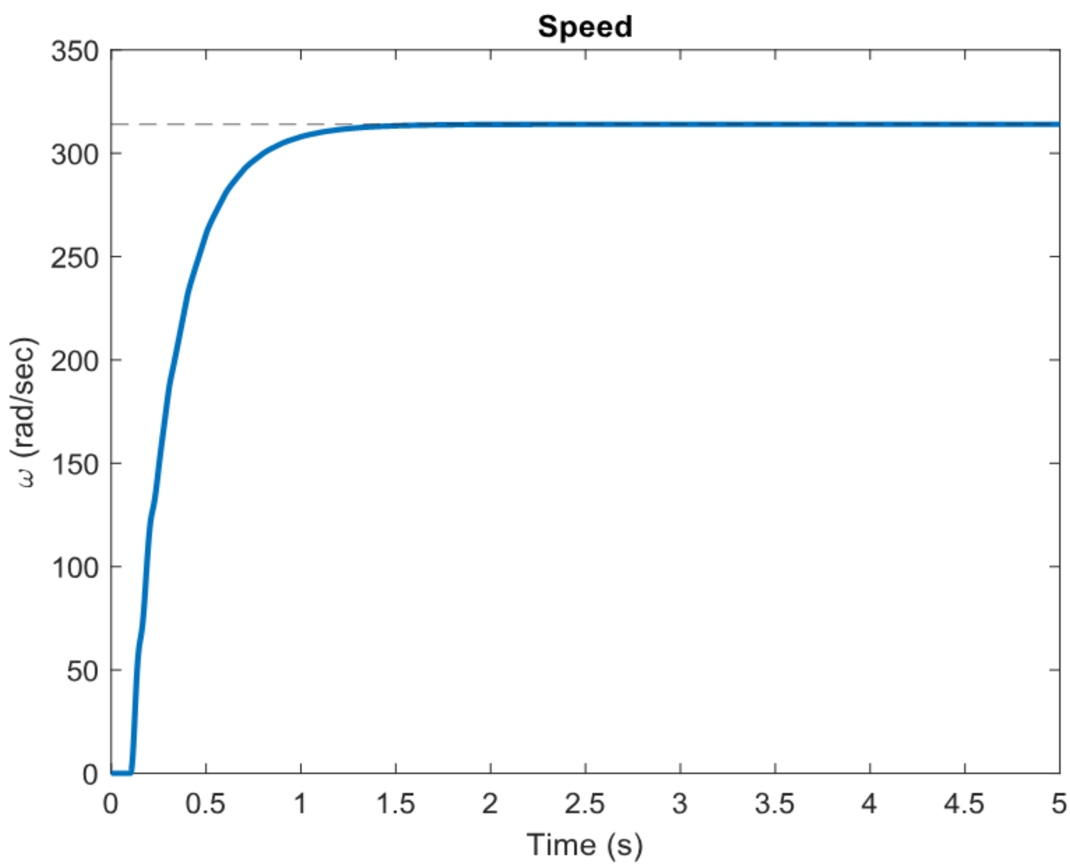

Figure 5.1 Reference Speed following Performance of NMPC.

Table 5.1 NMPC performance parameter results.

	Rise time(sec)	Settling time(sec)	Overshoot (%)	Steady state error
NMPC	0.4902	0.9922	0	0

Table 5.1 presents the performance of the NMPC controller. The rise time, i.e., the time taken by the response of the system to reach from 10% to 90% of its final value, is 0.4902 seconds, indicating fast dynamic response. The settling time of the system is 0.9922 seconds, i.e., the output settles down within the required tolerance band (generally ±2%) within a time less than one second, indicating proper damping of oscillations. Notably, the system is 0% overshoot, indicating that there is no overresponse following the final value, and the steady-state error is also 0, ensuring that the controller follows the reference input without long-term drift.

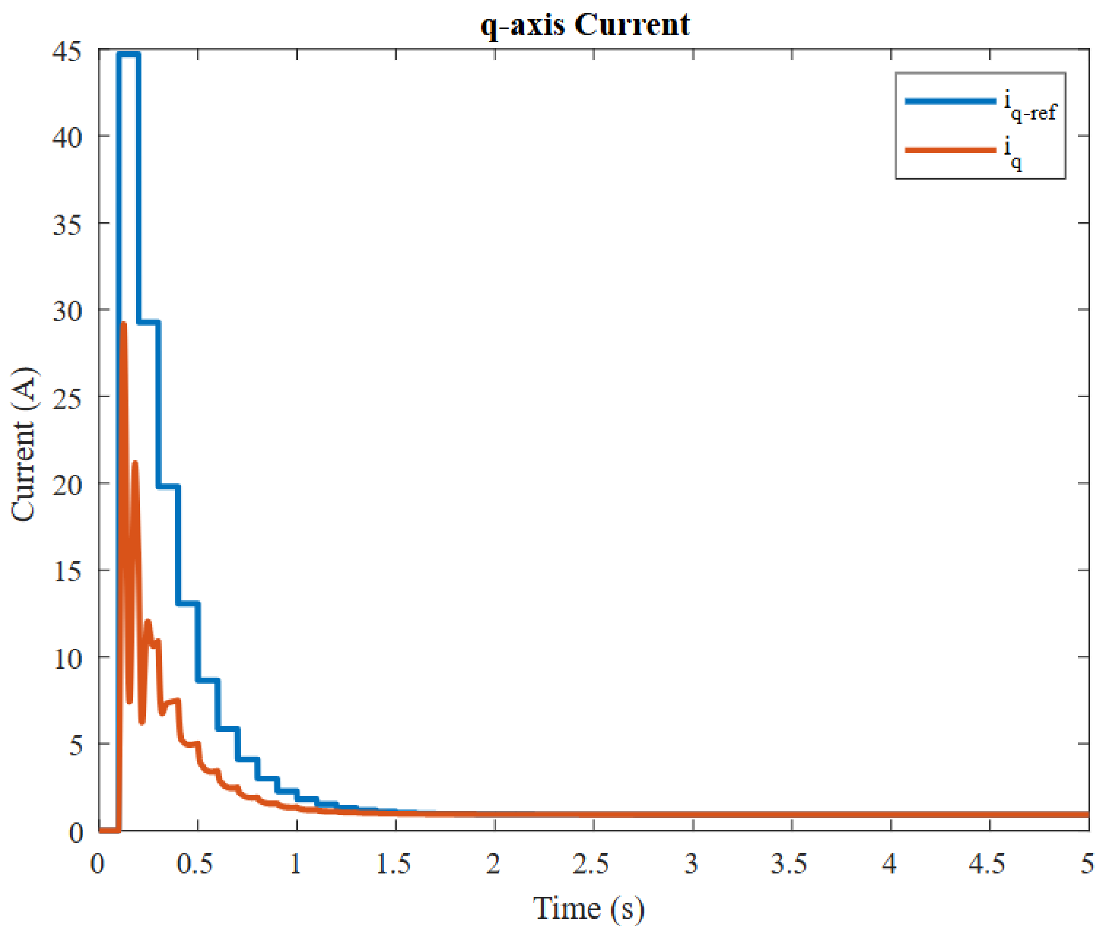

Figure 5.2 q-axis current response.

The plot of Figure 5.2 shows the behavior of the quadrature-axis current over time. In the motor control strategies, i_q is directly proportional to the torque produced by the motor. Therefore, this plot shows how the controller commands torque to achieve the desired speed.

The i_d plot in Figure 5.3 shows the PI controller's tracking performance after the NMPC's d-axis current reference. The NMPC computes a new i_{dref} every 0.1 s based on the system state, and then the PI controller tracks the reference at a much faster sampling time (0.001 s). In the result, we can observe that i_d closely follows the reference with minimal steady-state error and fast dynamic response speed, and this confirms that the inner-loop PI controller precisely provides the precise current control needed for the outer-loop NMPC to function properly. There may be minor oscillations due to the high update rate, but they are maintained within reasonable limits so the system remains stable and precise.

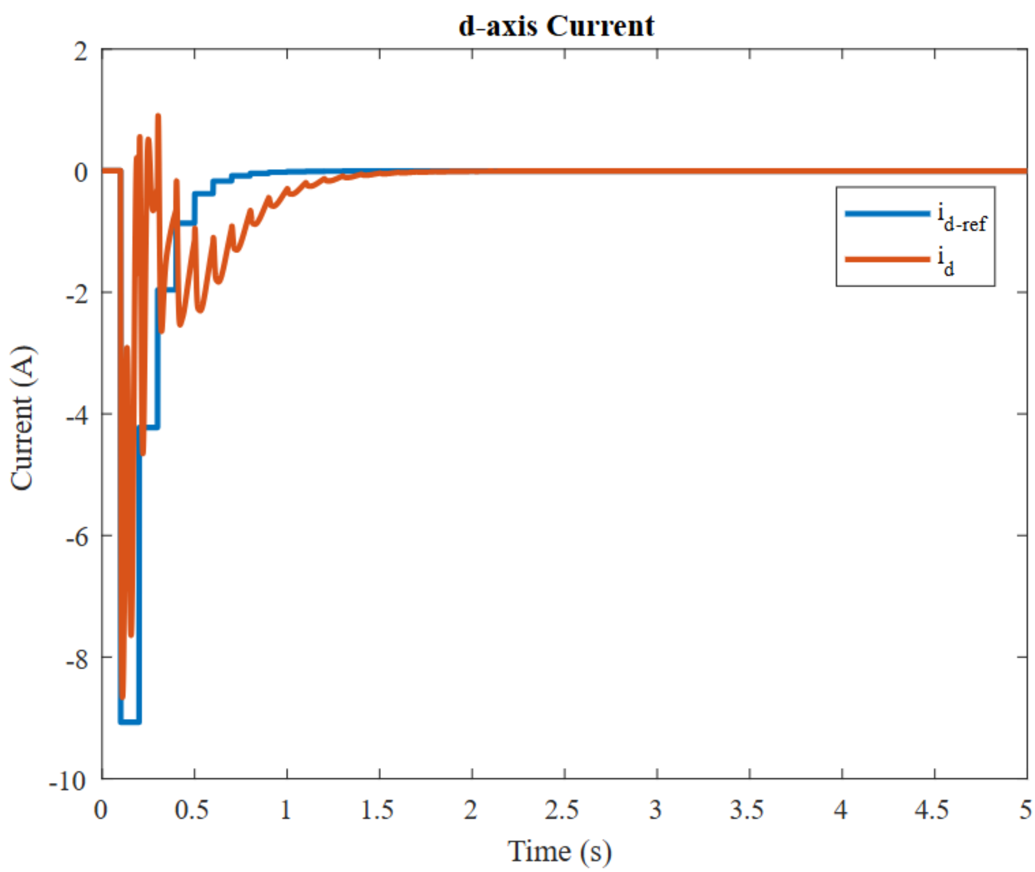

Figure 5.3 d-axis current response.

In the Figure 5.4, v_d gradually approaches zero as the system stabilizes. This behavior reflects that, at steady-state, the direct-axis voltage needed to maintain the desired i_d becomes negligible, meaning the flux control is balanced. On the other hand, v_q converges to a constant nonzero value, which is expected because v_q is directly responsible for sustaining the torque production. This steady v_q value ensures that the motor delivers the required torque to maintain the target speed set by the NMPC.

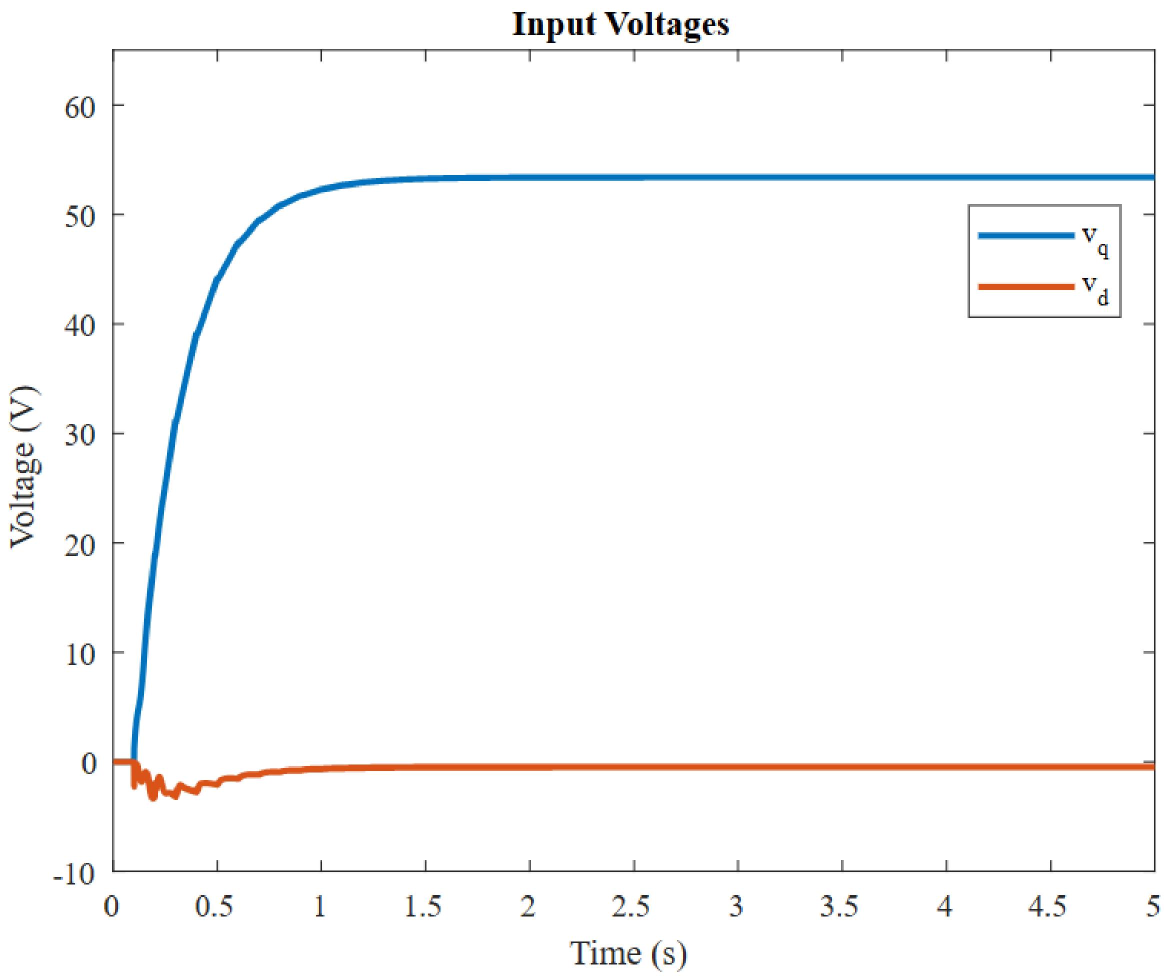

Figure 5.4 Input voltage V_d and V_q response.

5.2 NMPC Vs LMPC Setpoint speed tracking Comparison

In the speed tracking Figure 5.5, the reference speed is initially set to 314 rad/s, then reduced to 200 rad/s, and finally increased back to 314 rad/s. The performance of the NMPC and LMPC controllers is compared based on how accurately and quickly they track these changing reference values.

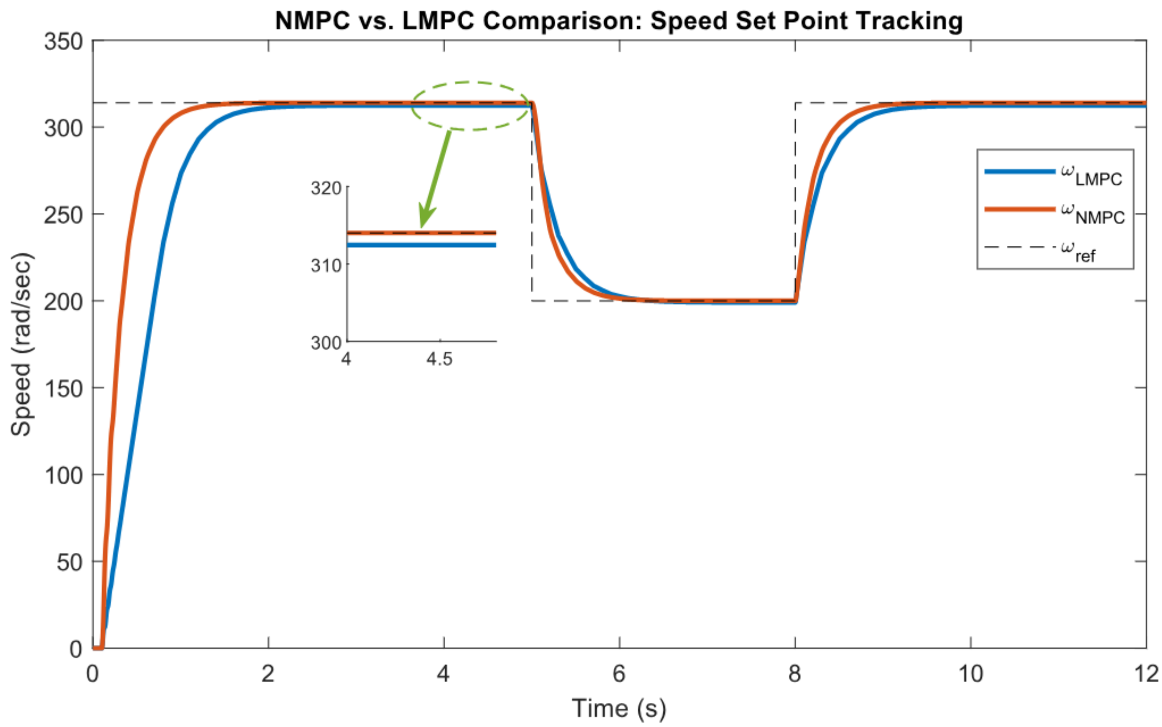

Figure 5.5 speed setpoint tracking comparison: NMPC vs LMPC.

Table 5.2 speed controller comparison of performance parameter results.

Speed controller	Performance metrics(parameters)			
	Rise time(sec)	Settling time(sec)	Overshoot (%)	Steady state error (%)
LMPC	0.8865	1.5363	0	1.5469
NMPC	0.4902	0.9922	0	0

In the Figure comparing NMPC and LMPC setpoint tracking, it is evident that NMPC outperforms LMPC in terms of both speed and accuracy. Specifically, NMPC achieves a rise time of 0.4902 seconds and a settling time of 0.9922 seconds, demonstrating faster convergence to the speed reference. Additionally, NMPC provides a smoother response with zero overshoot and zero steady-state error, indicating precise tracking performance.

In contrast, LMPC exhibits a slower rise time of 0.8865 seconds and a longer settling time of 1.5363 seconds. While it also maintains zero overshoot, it results in a steady-state error of 1.5469, reflecting a slight deviation from the desired speed. This deviation, particularly noticeable during transients, is attributed to the limitations of linearization in accurately predicting system behavior in nonlinear operating regions.

5.3 NMPC Vs LMPC Disturbance Rejection Comparison

An impulsive disturbance as a load torque was applied between the 5th to 8th second, simulating the case of ascending a hill when the vehicle was moving. Simulation results validate that NMPC is better to counteract the disturbance. Since the occurrence of the disturbance at the 5th second, NMPC responds immediately and begins to follow the reference speed with less deviation, validating good disturbance rejection properties.

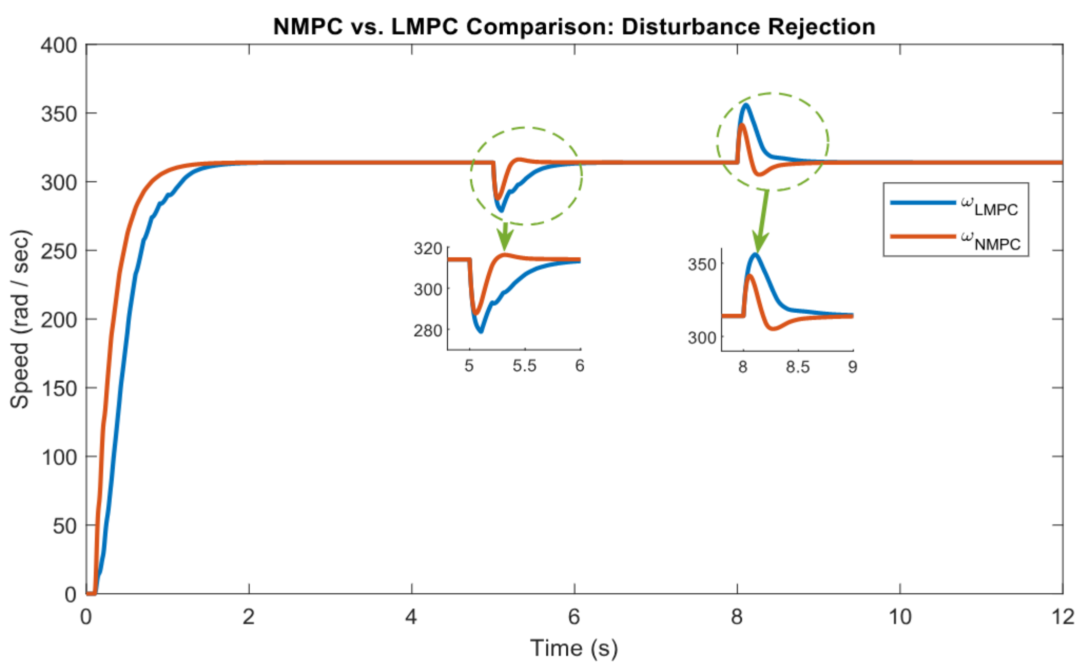

Figure 5.6 NMPC vs LMPC Disturbance Rejection Comparison.

In contrast, LMPC's response is slower, and the system experiences a visible lag while resisting the disturbance. The lag causes temporary degradation of tracking accuracy during the time of disturbance.

Once the disturbance is removed at the 8^{th} second (marking the vehicle at the hilltop), the two controllers experience a rapid overshoot as soon as the load torque returns to nominal. However, NMPC recovers faster and reaches the reference speed sooner than LMPC, again with the characteristic of slow convergence. Overall, the results show quite clearly NMPC's superiority in disturbance rejection and maintaining good tracking performance.

CHAPTER SIX

CONCLUSION AND RECOMMENDATION

6.1 Conclusion

This thesis presented the design and implementation of a Nonlinear Model Predictive Control (NMPC) method for speed control of an Interior Permanent Magnet Synchronous Motor (IPMSM) in electric vehicles (Hyundai Ioniq). The cascaded control structure was used with NMPC in the outer loop to calculate optimal current references and a PI controller with parameters tuned by a Genetic Algorithm (GA) in the inner loop to track these current references through voltage control.

The NMPC controller was compared to a typical Linear Model Predictive Control (LMPC) technique when tested under various speed reference profiles. Simulation results confirmed that the NMPC controller outperformed LMPC in terms of tracking performance. NMPC, specifically, provided faster response times, better disturbance rejection, and smaller steady-state errors during acceleration and deceleration phases. The NMPC performed well even under the nonlinearities in IPMSM dynamics, in which LMPC showed noticeable tracking delays and larger deviations.

Furthermore, voltages v_d and v_q were tested and exhibited as expected: v_d tended towards zero with time during effective flux weakening, and v_q settled to a value proportional to the torque reference. Controlled currents i_d and i_q followed behind their respective references well, advocating for the performance of the inner-loop PI controller.

Significantly, the utilization of various sampling periods 0.1 s for NMPC and 0.001 s for the PI controller enabled the system to reach high performance without sacrificing real-time feasibility. The rapid inner-loop updates guaranteed that the NMPC had accurate feedback every time it calculated the subsequent optimal control action.

In conclusion, the proposed NMPC approach with GA-tuned PI control provided significant improvements in speed tracking performance and energy-efficient operation of IPMSMs for EV drives. NMPC thereby provides a compelling solution to future advanced EV drive systems where high precision, robustness, and efficiency are requirements.

6.2 Recommendation

In order to further enhance the efficiency and performance of electric vehicles, Nonlinear Model Predictive Control (NMPC) needs to be more widely implemented in EV production. NMPC's superior predictive capabilities provide better speed tracking, enhanced handling of system constraints, and overall better drive system performance compared to traditional control approaches. With the progress of electric vehicles toward higher intelligence and efficiency, the use of NMPC in real-world production vehicles can make significant contributions to the realization of better dynamic response, stability, and maximum energy usage, and hence is a good candidate for future EV control systems.

Although the effectiveness of NMPC has been confirmed by simulation in this study, it is necessary to conduct hardware implementation to comprehensively prove its applicability in real-time systems. Future studies would include the implementation of the achieved NMPC method on real-time platforms. Experimental testing will allow researchers and engineers to experiment with real-time computing capability, disturbance rejection performance, and robustness across various operating conditions, thus facilitating a smoother transition from simulation to industrial applications.

Furthermore, the predictive capability of the NMPC can be made even more efficient by applying artificial intelligence (AI) methods. Machine learning, neural networks, and reinforcement learning are some of the methods that can be used to predict disturbances, driver behavior, or system uncertainties even better, hence enabling the controller to make even smarter and more responsive decisions. The combination of AI and NMPC offers a novel research field that can significantly improve control accuracy, system performance, and fault tolerance, further improving the reliability and intelligence of electric vehicle driving systems.

Research Fund Acknowledgement

This thesis work is funded by Adama Science and Technology University under grant number ASTU/SM-R/1109/25.

REFERENCE

Akhtar, M. J., Behera, R. K., & Parida, S. K. (2015, December). Propulsion system design of electric vehicle. In *2015 6th International Conference on Power Electronics Systems and Applications (PESA)* (pp. 1-5). IEEE.

Baral, S. K. (2021). Closed loop control of pmsm motor: Field oriented control using hall sensors.

Bello, A., Kilishi, I. M., Bari, M. M., & Abubakar, U. (2014). Comparative Review Of PMSM And BLDCM Based On Direct Torque Control Method. *International Journal of scientific & technology research*, *3*(3), 195-199.

Boby, K., & Kottalil, A. M. (2013). Simulation of PMSM Vector Control System with Fuzzy Self-Adjusting PID Controller Using MATLAB.https://api.semanticscholar.org/CorpusID:16942110

Butt, C. B., Hoque, M. A., & Rahman, M. A. (2004). Simplified fuzzy-logic-based MTPA speed control of IPMSM drive. *IEEE Transactions on industry applications*, *40*(6), 1529-1535.

Cao, W., … A. B.-… R. J. of, & 2019, undefined. (n.d.). Review of electrical motor drives for electric vehicle applications. Search.Informit.Org. https://doi.org/10.22581/muet1982.1903.01

Chai, S., Wang, L., & Rogers, E. (2013). Model predictive control of a permanent magnet synchronous motor with experimental validation. Control Engineering Practice, 21(11), 1584–1593. https://doi.org/10.1016/J.CONENGPRAC.2013.07.008

Colak, I., Kabalcı, E., & Bayindir, R. (2011). Review of multilevel voltage source invertertopologies and control schemes. Energy Conversion and Management, 52, 1114–1128.https://doi.org/10.1016/j.enconman.2010.09.006

Derammelaere, S., Haemers, M., De Viaene, J., Verbelen, F., & Stockman, K. (2016, November). A quantitative comparison between BLDC, PMSM, brushed DC and stepping motor technologies. In *2016 19th International Conference on Electrical Machines and Systems (ICEMS)* (pp. 1-5). Ieee.

Dong, G., Yang, J., Qiu, X., Liu, X., & Wei, C. (2018, October). Space Vector Flux Weakening Control of PMSM Drivers. In *IOP Conference Series: Earth and Environmental Science* (Vol. 192, No. 1, p. 012010). IOP Publishing.

El Fakir, C., El Idrissi, Z., Lassioui, A., Belhaj, F. Z., Gaouzi, K., El Fadil, H., & Rachid, A. (2023). Adaptive nonlinear control of salient-pole PMSM for hybrid electric vehicle applications: theory and experiments. *World Electric Vehicle Journal*, *14*(2), 30.

Gao, F., Liu, F., & Sidorov, D. (2018). Non-cascade speed and current control of IPMSM for electrical vehicles based on model predictive control. In ISCIIA and ITCA 2018-8th International Symposium on Computational Intelligence and Industrial Applications and 12th China-Japan International Workshop on Information Technology and Control Applications.

Grüne, L., & Pannek, J. (2011). Nonlinear Model Predictive Control. https://doi.org/10.1007/978-0-85729-501-9

Huang, X., Pan, H., & Yuan, K. (2020). Speed and Current Control of PMSM based on Double MPC. Proceedings - 2020 7th International Forum on Electrical Engineering and Automation, IFEEA 2020, 300–304. https://doi.org/10.1109/IFEEA51475.2020.00070

Hyundai Canada. (2024). *2024 IONIQ 5 specifications*. https://www.hyundaicanada.com/en/showroom/2024/ioniq-5/specs

Hyundai Motor Company. (2023, June 26). *2024 IONIQ 5 specifications*. Hyundai Newsroom. https://www.hyundainews.com/assets/documents/original/56233-2024IONIQ5Specs062623.pdf

Kim, Y., Lee, S., & Kim, J. (2013). The maximum efficiency driving in IPMSM by precise estimation of the linkage flux, inductance, and iron loss. *Journal of Electrical Engineering & Technology*, *8*(6), 1371–1378. https://doi.org/10.5370/JEET.2013.8.6.1371

Kebedew, M. H., & Kim, S. (2024). Improved Speed Control through Model Predictive Techniques for Permanent Magnet Synchronous Motor in Electric Vehicles. *Daagu International Journal of Basic and Applied research (DIJBAR)*, *6*(1), 435-450.https://doi.org/10.20372/dijbar67892.v6i1.2024

Krishnan, R. (1991). Application Characteristics of Permanent Magnet Synchronous and Brushless dc Motors for Servo Drives. IEEE Transactions on Industry Applications, 27(5), 986–996. https://doi.org/10.1109/28.90357

Kumar, K., Angel, P., John, J., & Kumar. (2010). Simulation and comparison of SPWM and SVPWM control for three phase inverter. ARPN Journal of Engineering and Applied Sciences, 5

Lee, S. T., & Tolbert, L. M. (2009, September). Analytical method of torque calculation for interior permanent magnet synchronous machines. In *2009 IEEE Energy Conversion Congress and Exposition* (pp. 173-177). IEEE. https://sci-hub.se/10.1109/ECCE.2009.5316263

Liang, W., Wang, J., Luk, P., Fang, W., & Fei, W. (2014). Analytical Modeling of Current Harmonic Components in PMSM Drive with Voltage-Source Inverter by SVPWM Technique. Energy Conversion, IEEE Transactions On, 29, 673–680. https://doi.org/10.1109/TEC.2014.2317072

Liu, D. (2008). Brushless DC Motors Made Easy.

Liu, F., Gao, F., Liu, L., & Sidorov, D. N. (2019). IPMSM speed and current controller for electric vehicles based on explicit MPC. *Journal of Advanced Computational Intelligence and Intelligent Informatics*, *23*(6), 1019-1026. From https://www.jstage.jst.go.jp/article/jaciii/23/6/23_1019/_article/-char/ja/

Li, L., & Liu, Q. (2019). Research on IPMSM drive system control technology for electric vehicle energy consumption. *IEEE Access*, *7*, 186201-186210.

Liu, X., Zhang, C., Li, K., & Zhang, Q. (2016). Nonlinear predictive high order sliding mode control for permanent magnet synchronous motor drive system. *Journal of Mathematics and Computer Science*, *16*(3), 402-411.

Lu, K., & Zhu, Z. Q. (2024, September). Comparative Stability Analysis of IPMSM and SPMSM Machines Under Flux-Weakening Control. In 2024 International Conference on Electrical Machines (ICEM) (pp. 1-7). IEEE.

Minyamer Gelawe, G. (2020). Artificial Intelligence Based Non-linear PID Speed and Current Control of Brushless DC Motor for Electric Vehicle Drive.(The Case of Bajaj Qute) (Doctoral dissertation, ASTU).

Morimoto, S., Sanada, M., & Takeda, Y. (2006). Mechanical sensorless drives of IPMSM with online parameter identification. *IEEE Transactions on Industry Applications*, *42*(5), 1241-1248.

Murakami, H., Honda, Y., Kiriyama, H., Morimoto, S., & Takeda, Y. (1999, October). The performance comparison of SPMSM, IPMSM and SynRM in use as air-conditioning compressor. In *Conference Record of the 1999 IEEE Industry Applications Conference. Thirty-Forth IAS Annual Meeting (Cat. No. 99CH36370)* (Vol. 2, pp. 840-845). IEEE.

Nguyen, A. T., Pham, T. V., & Hoang, T. L. N. (2024, August). Speed Controller Design for Interior PMSM Drive Based on Model Reference Adaptive Control Strategy in EV Applications. In *2024 9th International Conference on Applying New Technology in Green Buildings (ATiGB)* (pp. 1-6). IEEE.

Oubelaid, A., Taib, N., Nikolovski, S., Alharbi, T. E., Rekioua, T., Flah, A., & Ghoneim, S. S. (2022). Intelligent speed control and performance investigation of a vector controlled electric vehicle considering driving cycles. *Electronics*, *11*(13), 1925.

PC, U., Saji, D., Cleetus, G., & Chandy, J. A. (2024). Field Oriented Control (FOC) of Permanent Magnet Synchronous Motor (PMSM) Applied in Electric Vehicle (EV). *Manipal Journal of Science and Technology*, *9*(2), 6.

Rauth, S. S., & Samanta, B. (2020). Comparative Analysis of IM/BLDC/PMSM Drives for Electric Vehicle Traction Applications Using ANN-Based FOC. 2020 IEEE 17th India

Council International Conference, INDICON 2020. https://doi.org/10.1109/INDICON49873.2020.9342237

Rodriguez, J., Pontt, J., Silva, C., Correa, P., Lezana Illesca, P., Cortes, P., & Ammann, U. (2007). Predictive Current Control of a Voltage Source Inverter. Industrial Electronics, IEEE Transactions On, 54, 495–503. https://doi.org/10.1109/TIE.2006.888802

Ruan, G. Q., Su, Y. Y., Cao, J. L., Su, Y. H., Gong, Z. D., & Hu, X. (2025). Position tracking control of permanent magnet synchronous motor based on AHONFTSMC control. *Journal of Electrical Engineering & Technology*, *20*(1), 389-401.

Tan, K., Su, J., … H. W.-2020 T. 46th A. C. of, & 2020, undefined. (n.d.). MPC Based Full speed Domain Control Strategy of Interior Permanent Magnet Synchronous Motor. Ieeexplore.Ieee.Org. Retrieved April 19, 2023, from https://ieeexplore.ieee.org/abstract/document/9255410/

Thattil, A., Vachhani, S., Raval, D., Patel, P., & Sharma, P. (2019). Comparative study of using different electric motors for EV. *International Research Journal of Engineering and Technology (IRJET)*, *6*(4), 4601-4604.

Tian, M., Cai, H., Zhao, W., Energies, J. R.-, & 2023, undefined. (n.d.). Nonlinear Predictive Control of Interior Permanent Magnet Synchronous Machine with Extra Current Constraint. Mdpi.Com. Retrieved April 19, 2023, from https://www.mdpi.com/2056712

Uddin, M. N., & Rahman, M. A. (2007). High-speed control of IPMSM drives using improved fuzzy logic algorithms. *IEEE transactions on industrial electronics*, *54*(1), 190-199.

Wang, J., & Yu, D. (2023). Fuzzy controller-based predictive speed control of a permanent magnet synchronous motor. *Proceedings of the Indian National Science Academy*, *89*(4), 811-824.

Xin, X., & Chengning, Z. (2017). Optimal design of electric vehicle power system with the principle of minimum curb mass. *Energy Procedia*, *105*, 2629-2634.

APPENDICES

Appendix A: MATLAB Implementation for the Driving Power vs. Speed Analysis of the Hyundai Ioniq Vehicle.

```
m=2600; g=9.81; a=0.5;

R=0.37055; Ctrr=0.01; Cad=0.29;

Effieciency=0.95; den=1.23; Af=2.5704;

F_tot=0; Vkph=0; Vkph1=0; ang=0;

ang1=20; d_Vkph=1e-2; Vkph_fin=200;

y=1; t=1;

while (Vkph<Vkph_fin);

Vmps=Vkph*(1000/3600);

Theta=ang *(2*pi/360);

FA=0.5*den*Cad*Af*(Vmps)^2;

if Vkph<=100*d_Vkph

StatFric=0.1;

else

StatFric=0;

end

FRolling=m*g*(Ctrr+StatFric)*cos(Theta);

FGradient=m*g*sin(Theta);

F_tot=FRolling+Fa+FGradient+m*a;

power=F_tot*vmps/0.95;
```

```
Vkph=Vkph+d_Vkph;

Vkph1=Vkph1+d_Vkph;

if y >16

Powern(t)=Power/1000;

Vkphn(t)=Vkph;

t=t+1;

y=1;

end

y=y+1;

end

figure(1);

plot(Vkphn,Powern,'b','linewidth',1.5)

axis([0 200 0 200]);

%legend('Total force','Gradient Force','Rolling Force','Aerodynamic Force')

grid

title('Power verses Vehicle Speed of the in km/hr','Interpreter','Latex')

xlabel('Speed of the car(km/hr)','Interpreter','Latex')

ylabel('Power(kW)','Interpreter','Latex')
```

Appendix B: closed loop performance of NMPC

```
import casadi.*

% Parameters
```

```
nx = 2;      % Number of states

nu = 2;      % Control inputs (i_d, i_q)

nd = 1;      % Disturbance dimension (same as u for demo)

N = 10;      % Prediction horizon

dt = 0.1;   % Sampling time

sim_steps = 5;


Rs = 0.01;

p = 4; lambda = 0.17; Lq = 0.0016; Ld = 0.0008; b = 0.003;

J = 0.015;

% --- Dynamics with disturbance

x = SX.sym('x', nx);

u = SX.sym('u', nu);

d = SX.sym('d', nd);

xdot = (3*p*(lambda*u(1) + (Ld - Lq)*u(1)*u(2))/2 -  d - b*x) / J;  % Example: disturbance
affects state 2

f = Function('f', {x, u, d}, {xdot})

% --- RK4 Integrator with disturbance

rk4_with_dist = @(f, x, u, d, dt) ...

    x + dt/6*(f(x,x,d) + 2*f(x+dt/2*f(x,u,d),u,d) + ...

            2*f(x+dt/2*f(x+dt/2*f(x,u,d),u,d),u,d) + ...
```

```
          f(x+dt*f(x+dt/2*f(x+dt/2*f(x,u,d),u,d),u,d),u,d));

% Symbolic variables

X = SX.sym('X', nx, N+1);

dU = SX.sym('dU', nu, N);

P = SX.sym('P', 2 * nu + nu + nd*N);  % [x0; u_prev; d0...dN-1]

x0 = P(1:nx);

xs = P(nx+1:2*nx);

u_prev = P(2*nx+1:2*nx+nu);

d_pred = reshape(P(2*nx+nu+1:end), nd, N);  % Predicted/measured disturbances

% Reconstruct U from dU

U = SX.zeros(nu, N);

U(:,1) = u_prev + dU(:,1);

for k = 2:N

   U(:,k) = U(:,k-1) + dU(:,k);

end

% Objective and constraints

obj = 0;

g = [];

Q = 1;

R1 = diag([0.1, 0.1]); R2 = diag([0.1, 0.1]);

for k = 1:N
```

```
    xk = X(:,k);

    uk = U(:,k);

    x_next = rk4_with_dist(f, xk, uk, dk, dt);

    g = [g; X(:,k+1) - x_next];

    obj = obj + (xk-xs)'*Q*(xk-xs) + 0.1*uk'*R1*uk + 0.01*dU(:,k)'*R2*dU(:,k);

end

g = [g; X(:,1) - x0];

% Control constraints

u_min = [-100; -200];

u_max = [350; 0];

u_bounds = [];

for k = 1:N

    u_bounds = [u_bounds; U(:,k) - u_min; u_max - U(:,k)];

end

g = [g; u_bounds];

OPT_variables = [reshape(X, nx*(N+1), 1); reshape(dU, nu*N, 1)];

g_l = [zeros(nx*N + nx, 1); zeros(2*nu*N, 1)];

g_u = [zeros(nx*N + nx, 1); inf(2*nu*N, 1)];

du_min = repmat([-10; -2], N, 1);

du_max = repmat([10; 2], N, 1);

nlp = struct('x', OPT_variables, 'f', obj, g, 'p', P);
```

```
opts.ipopt.print_level = 0;

opts.print_time = 0;

solver = nlpsol('solver', 'ipopt', nlp, opts);

%% PI

e1 = 0; e2 = 0; z1 = 0; z2 = 0; ee1 = 0; ee2 = 0;

kp1 = 0.2438; kp2 = 0.0248; ki1 = 2.9024; ki2 = 6.5563; % 0.7138

% kp1 = 0.2438; kp2 = .4; ki1 = 2.9024; ki2 = 85.5563; % 0.7138

% kp1 = 0.0326; kp2 = 2.9461; ki1 = 0.0289; ki2 = 90.5973; % 0.7138

% kp1 = 0.0439; kp2 = 2.2946 ; ki1 =0.0197; ki2 = 936.7734; % 0.713

dt_pi = 0.001;

h = dt_pi;

%% --- Simulation Loop

x_sim = [0; 0; 0];

u_prev_val = [0; 0];

mpc_steps = 0;

u_apply = u_prev_val;

UU = []; U_out= []; tt = 0; time = [0];

X_log = zeros(nx, sim_steps);

U_log = zeros(nu * 2, sim_steps);

dU_log = zeros(nu, sim_steps);

X_log(:, 1) = x_sim(3);
```

```
dU_log(:, 1) = [0;0];

xs = 314;

UU = [0 0]; U_out= [0 0]; tt = 0; time = [0];

%%

for t = 1:5 / h

    if mpc_steps >= dt

        % Simulate or estimate current disturbance (could be noisy, dynamic, etc.)

        d_now = 0;  % Example: known disturbance

        d_pred_val = repmat(d_now, 1, N);        % Assume it's constant over horizon

        % Initial guesses

        X0 = repmat(x_sim(3), 1, N+1);

        dU0 = zeros(nu, N);

        args.x0 = [reshape(X0, nx*(N+1), 1); reshape(nu*N, 1)];

        args.lbx = [-inf*ones(nx*(N+1), 1); du_min];

        args.ubx = [ inf*ones(nx*(N+1), 1); du_max];

        args.lbg = g_l;

        args.ubg = g_u;

        args.p = [x_sim(3); xs; u_prev_val; reshape(d_pred_val, nd*N, 1)];

        % Solve

        sol = solver('x0', args.x0, 'lbx', args.lbx, ...

            'ubx', args.ubx, 'lbg', args.lbg, ...
```

```
                'ubg', args.ubg, 'p', args.p);
        w_opt = full(sol.x);
        dU_opt = reshape(w_opt(nx*(N)+1:end), nu, []);
        u_apply = u_prev_val + dU_opt(:,1);
        u_prev_val = u_apply;
        mpc_steps = 0;
end
d = 0;
mpc_steps = mpc_steps + h;
Id_ref = u_apply(2); Iq_ref = u_apply(1);
UU = [UU; Id_ref Iq_ref];
e1 = Id_ref - x_sim(1);
z1 = z1 + 0.5*h*(e1); ee1 = e1;
u1 = kp1*e1+ki1*z1;  % vd
e2 = Iq_ref - x_sim(2);
z2 = z2 + 0.5*h*(ee2+e2); ee2 = e2;
u2 = kp2*e2 + ki2*z2;  % vq
u = [u1; u2];   % vd and vq
U_out = [U_out; u(2) u(1)];
x_sim = RK4(@model, tt, x_sim, u, h, d);
% u_prev_val = [u2; u1];
```

```
        tt = tt + h;
        % Log
        X_log(:, t+1) = x_sim(3);
        U_log(:, t+1) = [u_apply; x_sim(1:2)];
        time = [time; tt];
        % dU_log(:, t+1) = dU_opt(:,1);
end
ss_error = norm((x_sim(8)-x), 2)
stepinfo(X_log(1, :)', time)
% --- Plot results
figure;
% subplot(3,1,1);
plot(time, X_log', LineWidth= 2), hold on
yline(xs, "--")
ylim([0, 350])
xlim([0, 5])
% legend('\omega');
title('Speed');
ylabel("\omega (rad/sec)")
xlabel('Time (s)');
% subplot(3,1,2);
```

```
figure

plot(time, U_log(1, :), LineWidth= 2), hold on

plot(time, U_log(4, :), LineWidth= 2), hold on

legend('i_q_{-ref}', 'i_q');

title('q-axis Current');

xlabel('Time (s)');

figure

plot(time, U_log(2, :), LineWidth= 2), hold on

plot(time, U_log(3, :), LineWidth= 2), hold on

legend('i_d_{-ref}', 'i_d');

title('d-axis Current');

xlabel('Time (s)');

ylabel('Current (A)')

figure

% subplot(3,1,3);

plot(time, U_out, LineWidth= 2);

legend('v_q', 'v_d');

title('Input Voltages');

xlabel('Time (s)'); ylabel("Voltage (V)")

ylim([-10, 65])

xlim([0, 5])
```

```
function xdot = model(t, x, u, d)

Rs = 0.01;

P = 4; lambda = 0.17; Lq = 0.0016; Ld = 0.0008; b = 0.003;

J = 0.015;

xdot = zeros(3, 1);

xdot(1) = (u(1) - Rs * x(1) + Lq * x(3) * x(2)) / Ld;

xdot(2) = (u(2) - Rs * x(2) - (Ld * x(1) + lambda) * x(3)) / Lq;

xdot(3) = (3*P*(lambda*x(2) + (Ld - Lq)*x(1) * x(2))/2 - d - b*x(3)) / J;

end
```